CHALMERS
UNIVERSITY OF TECHNOLOGY

# Feasibility study of IEEE 802.11ad for Vehicle-to-X communication

*Master of Science Thesis*

TAI HUANG

Department of Signals and Systems
*Division of Communication Systems*
CHALMERS UNIVERSITY OF TECHNOLOGY
Göteborg, Sweden, 2015

MASTER THESIS EX009/2016

# Feasibility study of IEEE 802.11ad for Vehicle-to-X communication

TAI HUANG


CHALMERS

Department of Signals and Systems
*Division of Communication Systems*
CHALMERS UNIVERSITY OF TECHNOLOGY
Göteborg, Sweden, 2015

Feasibility study of IEEE 802.11ad for Vehicle-to-X communication

TAI HUANG



Master Thesis EX009/2016

Department of Signals and Systems

Division of Communication Systems

Chalmers University of Technology

412 96 Gothenburg

Telephone +46705916662

Typeset in Word

Gothenburg, Sweden 2015

# Abstract

This thesis studies the Physical Layer (PHY) of the new IEEE 802.11ad Wireless Local Area Network (WLAN) standard and its feasibility for Vehicle-to-X (V2X) communication, which refers to vehicle-to-device communication and vehicle-to-infrastructure communication in this report. The current version of this standard was completed in 2012, and promises multi-gigabit throughput communication at short communication distances. It works in the unlicensed 60 GHz frequency band with much wider bandwidth. It employs higher order modulation schemes and supports Multiple-Input Multiple-Output (MIMO) beamforming to improve the communication performance. To understand the feasibility as well as the practical limitation of this standard for V2X communication, the standard for certain applications is evaluated in terms of link range, data throughput, packet error rate and coverage capability. The link range and the performance of MIMO beamforming are investigated by the use of mathematical models and Matlab simulations. The practical communication performance on physical (PHY) layer and MAC layer is measured in a real vehicle with the help of 802.11ad evaluation kits (EVKs). The results show the possibility of the implementation of this standard for the V2X communication. Meanwhile, the test outcomes also reflect some practical challenges on the implementation of this standard, such as large path loss, effects of human body, weak reflection gain and so on. As a result, many further investigations are still required.

***Keywords:*** IEEE 802.11ad, V2X communication, MIMO beamforming, very high data throughput, link range, measurement in the real vehicle

# Acknowledgement

This work was fully supported by the network design group at Volvo Cars Corporation. I would like to express my sincere appreciation to my manager Mr. Hans Alminger and Ms. Karin Nordin. I want to thank my supervisor Mr. Magnus Eek for giving me this opportunity to conduct this thesis work and for his help in the test phase. This project couldn't be completed without the guidance, help and patience of my supervisor Dr. Taimoor Abbas. Many thanks to him for all the time he devoted to help me. I am very grateful to my supervisor Mr. Mikael Nilsson for his constructive comments and questions on the thesis work.

I would like to thank my academic examiner Professor Erik Ström and my academic advisor Erik Steinmetz for their useful advice.

Finally, I want to thank Mr. Allen Heberling, the product manager of our evaluation kits supplier, for his effort to improve the evaluation kits and his valuable comments on the test results.

Tai Huang, Gothenburg, Sweden, 2015-10-28

# Content

# List of Figures

# List of Tables

# List of Abbreviations

| | |
|---|---|
| **EVKs** | Evaluation Kits |
| **BECM** | Battery Energy Control Module |
| **SRS** | Supplementary Restraint System |
| **WLAN** | Wireless Local Area Network |
| **PHY** | Physical layer |
| **MAC** | Medium Access Control |
| **V2X** | Vehicle-to-X (in this thesis X stands for the access points outside the vehicle or any other device inside the vehicle) |
| **AGC** | Automatic Gain Control |
| **STF** | Short Training Field |
| **CE** | Channel Estimation |
| **DMG** | Directional Multi-Gigabit |
| **SC PHY** | Single Carrier Physical layer frame |
| **LPSC PHY** | Low Power Single Carrier Physical layer frame |
| **OFDM** | Orthogonal Frequency Duplexing Modulation |
| **MCS** | Modulation Coding Schemes |
| **DBPSK** | Differential Binary Phase-Shifting Keying |
| **QPSK** | Quadrature Phase Shift Keying |
| **TRN-T** | Transmit training |
| **TRN-R** | Receive training |
| **TX** | Transmitter |
| **RX** | Receiver |
| **LOS** | Line Of Sight |

| | |
|---|---|
| **NLOS** | Non Line Of Sight |
| **PSDU** | Physical layer Service Data Unit |
| **ULA** | Uniform Linear Array |
| **UCA** | Uniform Circular Array |
| **DSSS** | Direct Sequence Spectrum Spreading |
| **LDPC** | Low Density Parity Code |
| **EIRP** | Equivalent Isotropically Radiated Power |
| **SISO** | Single Input Single Output |
| **MIMO** | Multiple Input Multiple Output |
| **EVB** | Evaluation Board |
| **CIS** | Central Information Screen |
| **RCPI** | Received Channel Power Indicator |
| **PER** | Packet Error Rate |
| **Rx_EVM** | Received single Error Vector Magnitude |
| **CPU** | Central Processing Unit |
| **MAC** | Medium Access Control |
| **MSDU** | MAC Service Data Unit |
| **FCS** | Frame Check Sequence |

# Chapter 1

# Introduction

Today, the Wireless Local Area Network (WLAN) technologies are widely adopted both in personal and industrial sectors. Especially, the WLAN is becoming the mainstream technology in automotive since its first implementation in 2008. Nowadays, the WLAN standards IEEE 802.11a/b/n/ac have been implemented for the connection between the vehicles and mobile devices **[1] [2]**, and the standard IEEE 802.11p that is valuable for vehicles' active safety is also into the phase of reality test in some countries. The IEEE 802.11 series of standards specifies the required technologies for implementing WLAN communication and provides the basis for wireless devices using WLAN bands. The growing requirement on communication performance promotes the continuous evolution of the 802.11 series of standards **[3]**.

In 2012, the new enhancement 802.11ad was released into market. It operates in the unlicensed 60 GHz band. It can support data rates up to 6.75 Gbps by using wide channels of 2.16 GHz, and thus could enable applications such as HD multi-media streaming inside a vehicle, high speed transferring of large files and so on.

## 1.1 Motivation

Nowadays, because of the development in electric and electronic systems, more and more automatic software (such as Battery Energy Control Module (BECM), Navigator, Supplementary Restraint System (SRS)) is being applied in vehicles. Most of this software requires frequent transfer of large size data files between vehicles and service centers. Moreover, the vehicle has become an important activity place in our daily life. The end-users have been setting higher expectation on their journey experience, e.g., multi-media entertainment (especially uncompressed video/audio), interaction games, etc. In order to realize these applications, a low latency and high throughout communication technology is required. Cables are often annoying for vehicle engineers, so the wireless solution is preferred whenever it is possible. Actually, due to the very large bandwidth and clear spectrum, the 60 GHz wireless communication including the IEEE 802.11ad technology has been the hot topic, especially for next generation high throughput wireless communication solution. Nowadays, the researchers have done much work on 60 GHz channel modeling and corresponding theoretical communication performance analysis in corridor/office environment and urban environment. Besides, some vendors have already achieved the very high throughput, low latency communication with their IEEE 802.11ad product in spacious indoor environment, e.g. office or living room. If possible, it will be of high value to implement this technology in vehicles. Therefore, this project investigates the feasibility of its implementation also on Vehicle-to-X (V2X) communication, which refers to

vehicle-to-device (V2D) communication and vehicle-to-infrastructure (V2I) communication in this report.

The study in this project is based on the specifications defined in the standard IEEE 802.11ad and the existing findings in the field of 60 GHz wireless communication. Comparing with other researches, this project mainly characterizes the communication performance in terms of data throughput, link range and coverage capability through both the theoretical analysis and the test in a real vehicle. As to my knowledge, this project is novel and nobody else has done this before. In addition, this thesis work also investigates the use cases of this technology in vehicles, and the hardware components and test tools supporting its practical implementation.

## 1.2 Thesis outline

Chapter 2 contains the background information of the IEEE 802.11 standard series and the introduction of IEEE 802.11ad. Chapter 3 presents the theoretical analysis of the features, which are important for the feasible implementation of IEEE 802.11ad on V2X communication. Chapter 4 introduces the test environment in a real car, the test equipment and the measurement results. Chapter 5 states the basic implementation plan of IEEE 802.11ad in vehicle and some use cases in the future. Conclusion and future work are presented in Chapter 6.

# Chapter 2

# Background

## 2.1 IEEE 802.11 series standards

The IEEE 802.11 standard series define the specifications for implementing the WLAN communication on the physical layer (PHY) and MAC layer. They are created and maintained by the IEEE 802 LAN/MAN standards committee. Today 802.11 based communication systems operate in unlicensed bands around 2.4, 3.6, 5 and 60 GHz. The descriptions of some popular enhancements are as follows.

### 802.11a

This standard was released in 1999. It operates in the 5 GHz band. With the implementation of 52-subcarriers Orthogonal Frequency Division Multiplexing (OFDM), it can support data rates up to 54Mbits/s **[4]**.

### 802.11b

This standard was released in early 2000. It operates in the 2.4 GHz band. The standard is a direct extension of Direct Sequence Spectrum Spreading (DSSS) technique. It can achieve data rates up to 11Mbits/s. However, the devices implementing this standard may suffer more interference because of many other devices operating in this band such as Bluetooth devices and microwave ovens **[5]**.

### 802.11g

This standard was released in 2003, and it combines the features of 802.11a and 802.11b. It operates in the 2.4 GHz band and implements the same OFDM scheme as the one in 802.11a. The data rate can reach up to 54 Mbits/s. It was rapidly adopted due to the reduction in production cost and desired higher throughput. The former dual band a/b product became the tri mode (a/b/g) **[6]**.

### 802.11n

This standard was completed in 2009. It operates in both the 2.4 GHz and 5 GHz bands. As compared with previous standards, it uses the Multi-Input-Multi-Output (MIMO) technology, and can thus support data rates up to 600Mbits/s **[7]**.

### 802.11ac

This standard was published in 2013 and is built on the standard 802.11n. It operates in the 5 GHz band but with wider channels (80 MHz in 802.11n vs. 160 MHz in 802.11ac), higher order modulation (64QAM in 802.11n vs. 256QAM in 802.11ac) and more spatial streams (4 in 802.11n vs. 8 in 802.11ac). Furthermore, an advanced MIMO technique (multi user-MIMO) is implemented for downlink. It also supports the optional technique such as transmit beamforming, space time block coding and so on. Theoretically, this standard should enable a data rate of at least 1Gbps **[8]**.

## 2.2 IEEE 802.11ad

This standard was published in 2012 and the first chipset was launched to market in 2014. The WLANs supporting this standard operate in the unlicensed 60 GHz band with much wider bandwidth channels, i.e., 2.16 GHz per channel. A high order modulation scheme (64QAM) and OFDM are implemented in this standard. It supports the optional MIMO-Beamforming technology. Theoretically, the raw data rate can reach up to 6.75 Gbps but at a lower power consumption rate.

### 2.2.1 Operation band

IEEE 802.11ad operates in the unlicensed band around 60 GHz including four channels defined in the standard. However, the practical situation varies geographically **[10]**. The detailed situations in major markets are shown in **Figure 1**. In this figure, a special case needs to be mentioned. Channel 2 and Channel 3 are available for WLAN in China, but the standard IEEE 802.11ad won't be applied in this market according to government policy. Instead, a new WLAN standard IEEE 802.11aj will take its place, which is built on the IEEE 802.11ad, but works in 45 GHz and 60 GHz dual bands with different channelization strategies.

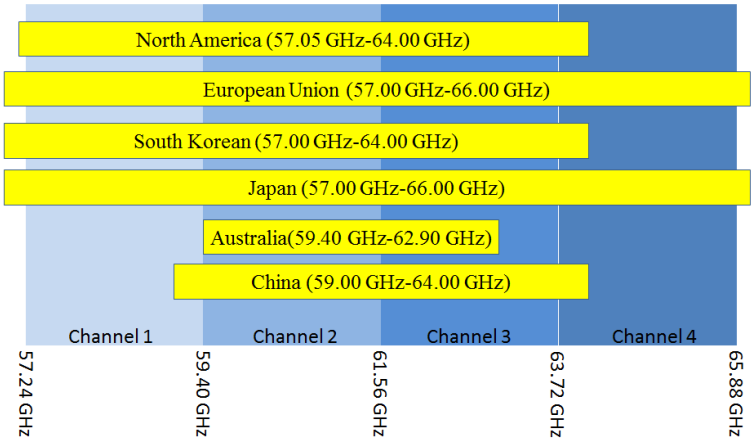


**Figure 1: Spectra available around 60 GHz**

### 2.2.2 Frame Structure

An 802.11ad PHY frame or so called Directional Multi Gigabit (DMG) PHY frame consists of a preamble, a header, data payload and optional training for beamforming **[10]**. A block diagram of the PHY frame structure is shown in **Figure 2**. The preamble field, which includes a short training field (STF) and a channel estimation (CE) field, is used for the packet detection, automatic gain control (AGC), frequency offset estimation and channel estimation. The following header field contains the important information for the receiver such as Modulation Coding Scheme (MCS), checksum and the length of the data field. After the header follows the data field, which carries the information data. The last part 'TRN', which is optional, consists of the training sequences for the beam refinement process.


**Figure 2: General structure of 802.11ad frame (source: [10])**

In order to fulfill different requirements, e.g. high throughput and robustness, the standard defines three types of modulations: spread-spectrum modulation, single carrier modulation and OFDM modulation. These three modulations correspond to four different PHY frame types: control PHY (CPHY), single carrier PHY (SCPHY), low power single carrier PHY (LPSCPHY), OFDM PHY. The structures of these 4 PHY frames are shown in **Figure 3**. The detailed description of each part in these PHY frames can be found in **[9]** and **[10]**.

Additionally, as shown in **Figure 3**, IEEE 802.11ad defines several different modulation schemes, which are applied in different PHY frames. For example, Differential Binary Phase Shift Keying (DBPSK) is only used in control frames and Quadrature Phase Shift Keying (QPSK) is only applied in OFDM frames. Meanwhile, $\frac{\pi}{2}-$BPSK is applied for the modulation of the preamble part in SCPHY, LPSCPHY and OFDMPHY. More details about these modulation schemes can be found in **[9]**.

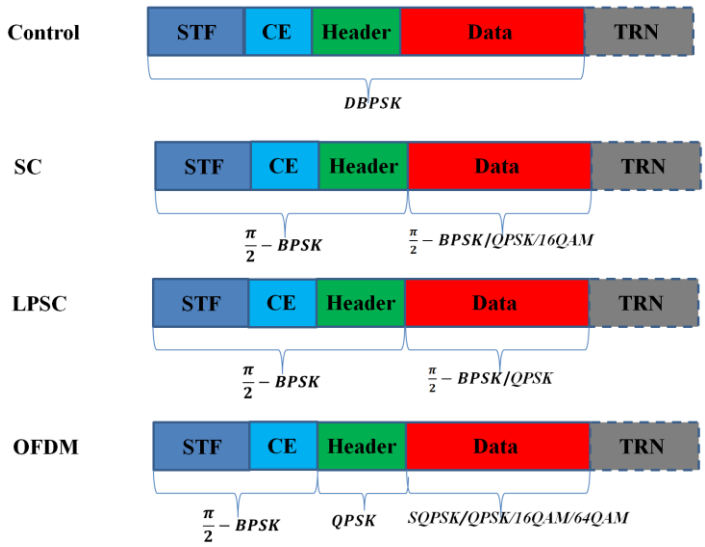


**Figure 3: Structures of 4 different frames (source: [10])**

### 2.2.3 Transmitter structure

For four different PHY frames mentioned in Section **2.2.2**, the block diagrams of data processing at transmitter side are shown in **Figure 4**. The details about each block can be found in **[9]**. As shown in these block diagrams, the standard also defines several different coding methods. The combination of different modulation scheme and different coding method will affect the communication performance such as data throughput, and Packet Error Rate (PER) at a certain SNR and communication distance.

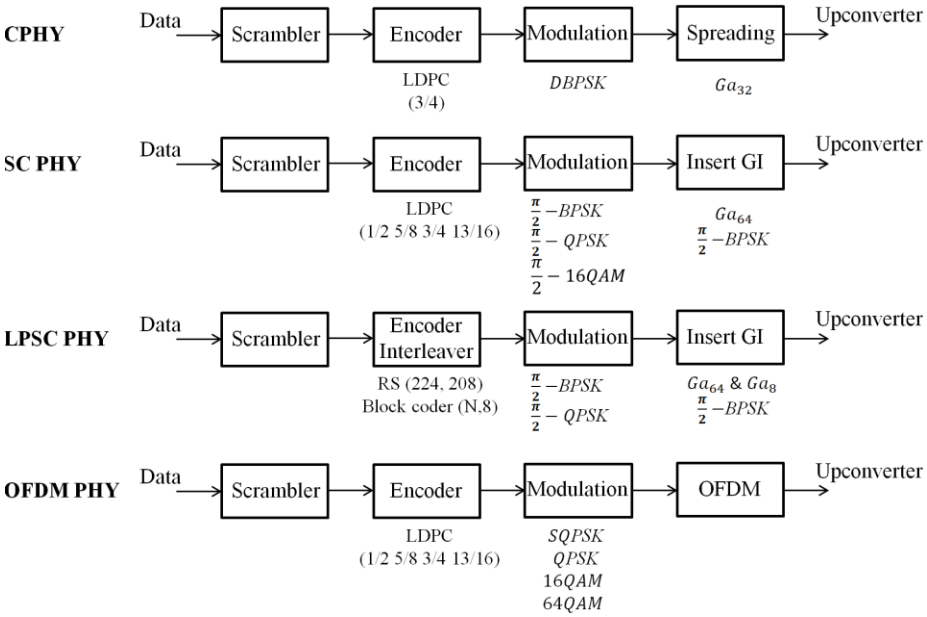


**Figure 4: Block diagram of data processing at Transmitter (source: [10])**

# Chapter 3

# Theoretical analysis

To determine the feasibility of IEEE 802.11ad for V2X communication, it is crucial to characterize the communication performance in terms of data throughput, link range and coverage capability. In addition, it is interesting to evaluate potential performance gains that can be achieved by using MIMO. In particular, how the layout and number of antennas affect the performance, as this can be valuable reference information for future design. In this Chapter, the theoretical analysis of these factors is presented.

## 3.1 Link range

The general link budget (in dB scale) of the wireless communication system is,

$$P_{\mathrm{r}} = P_{\mathrm{t}} + G_{\mathrm{t}} - L_{\mathrm{c}} + G_{\mathrm{r}} - P_{\mathrm{L}}, \quad (1)$$

where $P_{\mathrm{t}}$ is the transmit power, $P_{\mathrm{r}}$ is the receive power, $G_{\mathrm{t}}$ is the transmitter antenna gain, $G_{\mathrm{r}}$ is the receiver antenna gain, $L_{\mathrm{c}}$ is the cable loss and $P_{\mathrm{L}}$ is the path loss.

### 3.1.1 Transmit Power

The regulatory bodies in major markets around the world have already set regulations for 60 GHz operation. **Table 1** shows the summary of the specifications for the transmit power and the Equivalent Isotropically Radiated Power (EIRP) is shown in, which in dB scale can be modeled as EIRP $= P_{\mathrm{t}} + G_{\mathrm{t}} - L_{\mathrm{c}}$. For example, according to the regulation file from FCC, the upper limit for the transmit power is 27 dBm and the upper limit for the EIRP is 40 dBm **[11]**. In order to simplify the following analysis, the cable loss $L_{\mathrm{c}}$, the transmit antenna gain $G_{\mathrm{t}}$ and the receive antenna gain $G_{\mathrm{r}}$ are assumed to be 0, and the transmit power $P_{\mathrm{t}}$ is assumed to be 27 dBm.

**Table 1: The upper limits on transmit power and EIRP in major markets (Source: [12])**

| Country | EIRP (dBm) | Transmit Power (dBm) |
|---|---|---|
| Korea | 27 | 10 |
| Australia | 51.7 | 10 |
| Japan | 58 | 10 |
| USA/ Canada | 40 | 27 |
| European Union | 55 | 13 |

### 3.1.2 Path loss

In a realistic multi-path environment, the path loss $P_L$ in dB scale can be modeled as,

$$P_L(d) = P_L(d_0) + 10\,n\log_{10}\left(\frac{d}{d_0}\right) + \Psi_\sigma\,; d \geq d_0, \quad (2)$$

where $d$ is the distance, $n$ is path loss exponent, $P_L(d_0)$ is the path loss at the reference distance $d_0$, which is assumed to be 1 meter in this section and $\Psi_\sigma$ is a random variable describing the large-scale fading. The large scale fading $\Psi_\sigma$ can be described by a log normal distribution, which corresponding to a zero-mean Gaussian distribution with standard deviation $\sigma$ in dB domain, $\Psi_\sigma \sim N(0, \sigma^2)$.

This thesis investigates the feasibility of the standard IEEE 802.11ad for vehicle-to-infrastructure communication and vehicle-to-device communication, so both the outdoor channel model and indoor channel model are considered in this section.

1. The path loss model in outdoor channel
   The outdoor channel model is assumed for the communication between the vehicle and the infrastructure. Since transmission in the 60 GHz band is very sensitive to rain and snow, the path loss due to these weather conditions should also be considered in addition to the model in ( 2 ). To simplify the analysis, only one specific condition (heavy rain with precipitation rate of 25mm/hour) is studied in this report. The extra propagation loss due to this weather condition is about 10dB/km **[13]**, which means that the path loss for a heavy rainy day can be expressed as,

$$P_L = P_L(d_0) + 10\,n\log_{10}\left(\frac{d}{d_0}\right) + \Psi_\sigma + 10\left(\frac{d}{1000}\right). \quad (3)$$

   The path loss parameters $P_L(d_0)$, $n$ and $\Psi_\sigma$ depend on the environment, which can be classified into two scenarios: LOS and NLOS.

   a. LOS scenario

$$P_L(d_0) = 20\log_{10}\left(\frac{4\pi d_0}{\lambda}\right), \quad (4)$$

      where the wavelength $\lambda$ amounts to $0.005$m at 60 GHz. In **[15]**, based on the measurement of peer-to-peer link in urban environment, $n$ is estimated to be 2.25 and $\sigma$ is estimated to be 2 dB. In the following section, the link range in outdoor LOS channel is calculated based on these values.

   b. NLOS scenario
      The link range calculation in the following section will not consider this situation because of two reasons. First, there is no accurate data of path loss parameters of

outdoor NLOS channel. Second, NLOS situation is not common for practical use cases of outdoor vehicular WLAN communication.

2. The path loss model in indoor channel

For indoor channel, the mathematic model in ( 2 ) is used to calculate the path loss. The typical values of path loss parameter for the indoor channel in both LOS and NLOS scenarios have been reported in **[16]**. The information is summarized in **Table 2**.

**Table 2: Path-loss parameter values of indoor channel**

**(**The reference distance $d_0$ is 1 meter**)**

| Environment | LOS/NLOS | $P_L(d_0)$ [dB] | n | σ[dB] |
|---|---|---|---|---|
| **Conference** | LOS | 34~68.6 | 1.33~1.7 | 0.79~1.6 |
| **Computer** | LOS | 45.47 | 1.92 | 1.72 |
| **Office** | LOS | 34.8~84.6 | 0.56~2.1 | 1.2~5.4 |
| | NLOS | 34.8~56.1 | 3.5~3.74 | 3.9~8.6 |
| **Office/conf.** | LOS & NLOS | 70 | 1.33 | 5.1 |
| **Office/hall** | LOS | 70 | 2.17 | 0.88 |
| | NLOS | | 3.01 | 1.55 |
| **Laboratory** | LOS | 40.26~68.3 | 1.2~2.5 | 1.8~2.7 |
| | NLOS | 34.8 | 5.4 | 3.9 |
| **Corridor** | LOS | 50.65~74.05 | 1.87~2 | 0.14~2.3 |
| | NLOS | 70 | 1.64 | 2.53 |
| **Residential** | LOS | 56.1~75.1 | 1.53~1.73 | 1.5~1.6 |
| | NLOS | 86 | 2.44 | 6.2 |
| **Various** | LOS & NLOS | 50.65~69 | 1.88~2.1 | 7.9~8.6 |

As shown in **Table 2**, $P_L(d_0)$ ranges from 34 to 86 dB in LOS situations. However, at short transceiver distance of 1 meter the LOS component should be dominant when compared with other multipath components **[16]**, and thus the value of $P_L(d_0)$ is expected to be close to the value of 68 dB based on the free space law ( 4 ). The explanation for lower values of $P_L(d_0)$ in **Table 2** is that the antenna gain values might have not been removed in many cases, and the explanation for higher values of $P_L(d_0)$ is that the loss from the measurement equipment or the antenna misalignment might have not been taken into account. As a result, the most reasonable value of $P_L(d_0)$ in LOS scenario should be 68 dB as mentioned previously.

However, in NLOS scenario, the free space law can't be used to obtain the value of $P_L(d_0)$. Instead, it can be calculated as **[17]**,

$$P_L(d_0) = P_L(d_0)_{free} + P_L(d_0)_{diff} + P_L(d_0)_R , \quad (5)$$

where $P_L(d_0)_{free}$ is free space path loss, $P_L(d_0)_{diff}$ is diffraction loss, which refers to the attenuation from obstacles and $P_L(d_0)_R$ is the ground reflection loss. As shown in **Figure 5**,

one obstacle, which is approximated by a rectangular screen, is placed vertically and perpendicularly to the LOS path between the transmitter (TX) and receiver (RX). The diffraction loss from this object can be modelled by the simple sharp knife edge diffraction model for 4 edges of the screen **[18]**, which can be expressed as,

$$P_{\mathrm{L}}(d_0)_{\mathrm{diff}} = -20\log_{10}\left[1-\left(F_{\mathrm{h}_1}+F_{\mathrm{h}_2}\right)\left(F_{\mathrm{w}_1}+F_{\mathrm{w}_2}\right)\right], \quad (6)$$

where $F_{h_1}, F_{h_2}$ and $F_{w_1}, F_{w_2}$ account for the diffraction at 4 edges corresponding to the height *h* and the width *w* of the screen (shown in **Figure 5**), which is calculated as **[18]**,

$$F = \frac{\mathrm{atan}\left(\frac{\pi}{2}\sqrt{\frac{\pi}{\lambda}(D_1+D_2-r)}\right)}{\pi}, \quad (7)$$

where *r* is the transceiver distance which equals to $d_0$, $\lambda$ is the wavelength, $D_1$ and $D_2$ are the projected distances between the transmission terminals and each edge of the screen. As shown in **Figure 5**, $D_{1_{h_1}}, D_{1_{h_2}}, D_{1_{w_1}}$ and $D_{1_{w_2}}$ account for the projected distances between the transmitter and 4 edges corresponding to the height *h* and the width *w* of the screen. $D_{2_{h_1}}, D_{2_{h_2}}, D_{2_{w_1}}$ and $D_{2_{w_2}}$ are the projected distances between the receiver and 4 edges of the screen. The equation ( 7 ) is valid only when $D_1, D_2 \gg h_1,\ h_2,\ w_1,\ w_2$ and $D_1, D_2 \gg \lambda$. Therefore, in order to simplify the calculation, the rectangular obstacle is assumed to be at the central position of the LOS link between the transmitter and the receiver, the transceiver distance is $d_0$ equaling to 1 meter, and then $h_1, h_2, w_1$ and $w_2$ are assumed to be 5 cm.

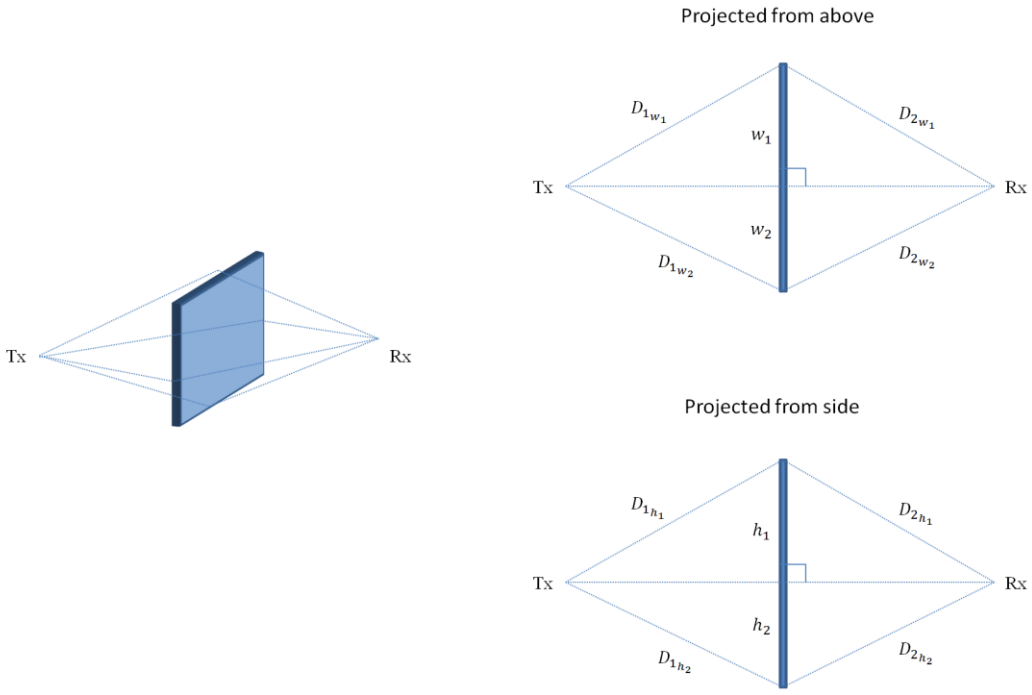


**Figure 5: Obstacle screen model**

According to **[17]**, the knife edge type of obstacles can reduce the ground reflection loss significantly. As a result, in indoor NLOS channel, $P_{\mathrm{L}}(d_0 = 1\ \mathrm{m})$ can be approximated as,

$$P_{\mathrm{L}}(d_0) \approx P_{\mathrm{L}}(d_0)_{\mathrm{free}} + P_{\mathrm{L}}(d_0)_{\mathrm{diff}} = 76.15\ \mathrm{dB}\,. \quad (8)$$

### 3.1.3 Link Range

For different MCS, the standard defines specific receiver sensitivity $S_{\mathrm{r}}$, which is from -68 dBm to -47 dBm under the condition of 5 dB implementation loss and 10 dB noise figure at receiver circuit **[9]**. The receiver sensitivity is defined as the minimum level of received signal required for a PER of 1% for a Physical layer Service Data Unit (PSDU) of 4096 octets. In other words, the received power $P_{\mathrm{r}}$ is required to be larger than $S_{\mathrm{r}}$ to satisfy the requirement on PER in the standard. The link range for a Single-Input-Single-Output (SISO) system, and different MCSs and different channel models, can thus be calculated based on the defined receiver sensitivity, and the assumptions in Section **3.1.1** and Section **3.1.2**. The link ranges obtained for different MCSs and different channel models are summarized in **Table 3**.

In the outdoor LOS channel, as can be seen in **Table 3**, the link range is no larger than 13 meters. Besides, according to the calculated results, the performance degrades a little bit in a rainy day, but not serious for short range communication. However, in practice, the performance can be improved with better antennas or better design of receiver circuit.

For the indoor channel, if LOS path exists, the link range is larger than 7 meters. Typically, the link range in indoor channel inside building environment is estimated to be more than 400m in low throughput transmission mode. Such a large value is due to the very small value of path loss exponent (0.56 in **Table 2**), which indicates the strong multipath propagation effect in a specific environment. If no LOS path exists, the performance degrades significantly and the very high throughput communication is not available. In addition, when applying the MCSs for low throughput communication, the link range is no larger than 13 meters. However, as visible in **Table 2**, the work on 60 GHz indoor channel modeling has been done in corridor environment or in office environment and the model for interior vehicles is missing. As a result, the calculated indoor link range just gives an overview on how 60 GHz channels behave and may not be valid in interior vehicle environment. Therefore, the measurement in a real vehicle is necessary for further investigation.

**Table 3: Link range for different MCS**

**(**Green represents the mandatory MCS, blue means the optional MCS and light green means these MCSs must be supported if OFDM is applied**)**

| | | | Link Range (m) | | | |
|---|---|---|---|---|---|---|
| | MCS index | Data rate (Mbps) | Outdoor LOS | Outdoor LOS (rainy) | Indoor LOS | Indoor NLOS |
| C_PHY | 0 | 27.5 | 35.9 | 34.7 | > 400 | 61.1 |
| SC_PHY | 1 | 385 | 12.9 | 12.7 | > 400 | 10.8 |
| | 2 | 770 | 10.5 | 10.4 | > 400 | 7.6 |
| | 3 | 962.5 | 8.6 | 8.5 | > 400 | 5.4 |
| | 4 | 1155 | 8.6 | 8.5 | > 400 | 5.4 |
| | 5 | 1251.25 | 7.0 | 6.9 | > 400 | 3.8 |
| | 6 | 1540 | 7.7 | 7.7 | > 400 | 4.5 |
| | 7 | 1925 | 7.0 | 6.9 | > 400 | 3.8 |
| | 8 | 2310 | 6.3 | 6.3 | > 400 | 3.2 |
| | 9 | 2502.5 | 5.1 | 5.1 | > 400 | 2.3 |
| | 10 | 3080 | 3.4 | 3.4 | 193 | 1.1 |
| | 11 | 3850 | 3.1 | 3.1 | 127 | NA* |
| | 12 | 4620 | 2.8 | 2.8 | 84 | NA |
| OFDM_PHY | 13 | 693 | 10.5 | 10.4 | > 400 | 7.6 |
| | 14 | 866 | 8.6 | 8.5 | > 400 | 5.4 |
| | 15 | 1386 | 7.7 | 7.7 | > 400 | 4.5 |
| | 16 | 1732 | 7.0 | 6.9 | > 400 | 3.8 |
| | 17 | 2079 | 5.7 | 5.7 | > 400 | 2.7 |
| | 18 | 2772 | 4.6 | 4.6 | > 400 | 1.9 |
| | 19 | 3465 | 3.8 | 3.8 | 291 | 1.3 |
| | 20 | 4158 | 3.1 | 3.1 | 127 | NA |
| | 21 | 4504 | 2.8 | 2.8 | 84.8 | NA |
| | 22 | 5197.5 | 2.3 | 2.3 | 37.3 | NA |
| | 23 | 6237 | 1.8 | 1.8 | 16.4 | NA |
| | 24 | 6756.75 | 1.5 | 1.5 | 7.2 | NA |
| LPSC_PHY | 25 | 626 | 8.6 | 8.5 | > 400 | 5.4 |
| | 26 | 834 | 5.7 | 5.7 | > 400 | 2.7 |
| | 27 | 1112 | 4.2 | 4.2 | > 400 | 1.6 |
| | 28 | 1251 | 4.2 | 4.2 | > 400 | 1.6 |
| | 29 | 1668 | 4.2 | 4.2 | > 400 | 1.6 |
| | 30 | 2224 | 4.2 | 4.2 | > 400 | 1.6 |
| | 31 | 2503 | 4.2 | 4.2 | > 400 | 1.6 |

* The calculated link range is smaller than the reference distance, which is not valid for the applied path loss model. As a result, it's shown as 'NA'.

## 3.2 MIMO

The discussion in the previous section implies that the link range might be the potential problem for V2X communication when applying the standard IEEE 802.11ad. To handle this issue, MIMO technology could be a good option, which uses multiple antennas at both the transmitter side and the receiver side to exploit multipath propagation. As shown in **Figure 6**, the transmitted signal reaches the receiver side through several links with different angles at different times. The transmission in each link experiences different fading and time delay. MIMO technology combines the signal from different links together with some specific algorithms. Through this process, it can reduce fading effects and optimize the data throughput without adding bandwidth or extra transmission power. Nowadays, the algorithms applied in MIMO system are divided into 3 main categories: beamforming, space time coding and spatial multiplexing. In what follows, the beamforming technique, which is widely used in IEEE 802.11n/ac as well as in IEEE 802.11ad, will be described.

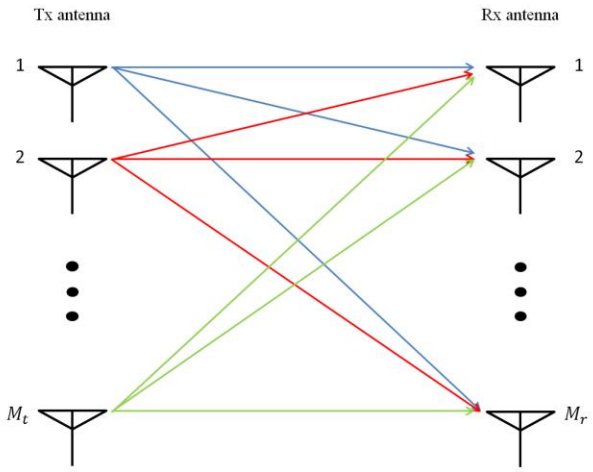


**Figure 6: Example of MIMO system**

### 3.2.1 Beamforming

According to **[9]**, beamforming is the MIMO technology defined in the standard IEEE 802.11ad. It's a signal processing algorithm, which generates a specific spatial beam to improve signal transmission and reception performance.

The multi path channel shown in **Figure 6** can be represented by a $M_r \times M_t$ matrix **H**. In order to simplify the analysis, Singular Value Decomposition (SVD) can be used to factorize **H** into three matrices. These matrices include two orthogonal matrices and one diagonal matric that contains the singular values of **H**. Through the SVD operation, the matrix **H** is expressed as,

$$\boldsymbol{H} = \boldsymbol{U\Sigma V}^{\mathrm{H}}, \qquad (9)$$

where

**U** is a $M_\mathrm{r} \times M_\mathrm{r}$ unitary matrix;

**V** is a $M_\mathrm{t} \times M_\mathrm{t}$ unitary matrix;

$\boldsymbol{\Sigma}$ is a $M_\mathrm{r} \times M_\mathrm{t}$ diagonal matrix. The rank of this matrix is $R_\mathrm{H} \leq \min(M_\mathrm{r}, M_\mathrm{t})$;

Based on the properties of the unitary matrices, the MIMO channel matrix can be decomposed into $R_\mathrm{H}$ equivalent parallel SISO channels through precoding with $\boldsymbol{V}$ at the transmitter side and shaping with $\boldsymbol{U}^H$ at the receiver side (shown in **Figure 7**). Each singular value in $\Sigma$ matrix corresponds to the gain factor of each parallel channel.

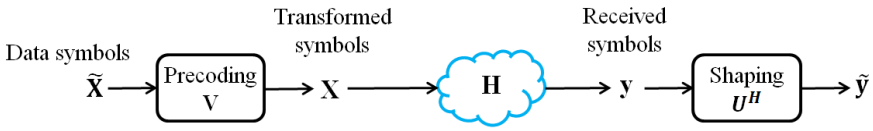


**Figure 7: Block diagram of SVD processing in MIMO**

$$\tilde{y} = \boldsymbol{U}^{\mathrm{H}}\boldsymbol{U}\boldsymbol{\Sigma}\boldsymbol{V}^{\mathrm{H}}\boldsymbol{V}\tilde{X} \qquad (10)$$

Beamforming is based on the parallel decomposition above. All the transmitters send the same symbol at the same time (shown in **Figure 8**), but with different weight factors and different phase shifts. The weight vectors **v** and **u** are chosen in **V** and **U** respectively along the largest singular value in $\boldsymbol{\Sigma}$. In this way, the signal is strengthened in the direction, where the channel gain is strongest. It can increase SNR at the receive side, and thus can improve the link range summarized in **Table 3**.

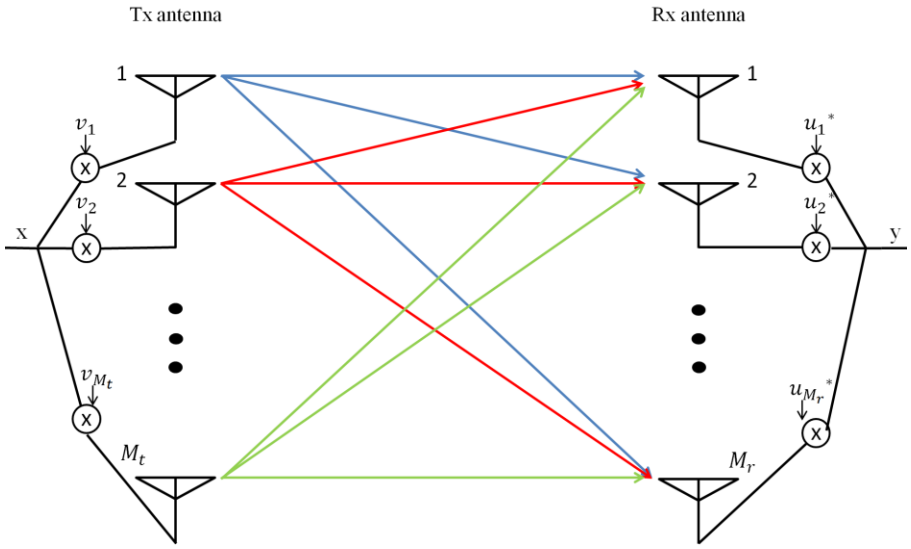


**Figure 8: Beamforming in MIMO**

### 3.2.1.1 Antenna array

As discussed before, MIMO beamforming could be valuable to improve the communication performance in bad channels with low SNR. Moreover, the standard IEEE 802.11ad has an advantage when applying this technology. Since any two radiating elements in antenna array should be spaced by at least half wave length, the shorter wave length (5 mm) in 60 GHz band, allows more antennas to be placed within a small space, as shown in **Figure 9**.

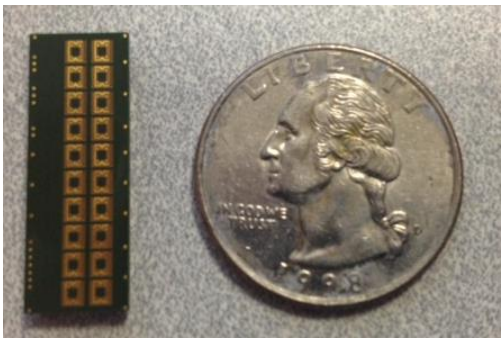

**Figure 9: The practical size of 16 elements antenna array on 60 GHz band (source: [21])**

In the standard IEEE 802.11ad, the header of every frame reserves 5 bits which indicates the number of beamforming training fields used in the communication. The standard should support $2^{\wedge}5 = 32$ beams or 32 antennas at each of the Tx and Rx side. In theory, this means that 32×32 MIMO systems can be used.

### 3.2.1.2 MIMO-OFDM Beamforming

As can be seen in **Table 3**, OFDM is the main technique for very high throughput communication, at least at short distances. However, if applying OFDM together with MIMO beamforming, the very high throughput communication can be achieved at longer distances, and thus MIMO-OFDM Beamforming is investigated in this section. The mathematical model of the system is shown in **[22]**. The received baseband signal at the *m*th subcarrier $y_m$ is given by,

$$y_m = \widetilde{H}_m x_m + n_m, \qquad m = 1 \dots N \tag{11}$$

where $x_m$ is the transmitted signal at the *m*th subcarrier, $n_m$ is a zero mean Gaussian noise vector with $\sigma^2$ variance, $N$ is the number of subcarriers, and $\widetilde{H}_m$ refers to the frequency response of the equivalent channel matrix after beamforming at the *m*th subcarrier, which can be expressed as,

$$\widetilde{H}_m = C^{\mathrm{H}} H_m W, \qquad m = 1 \dots N \tag{12}$$

where $C^{\mathrm{H}}$ is a shaping vector at the receiver side, $W$ is a precoding vector at the transmitter side and $H_m$ is the frequency response of MIMO channel matrix at the *m*th subcarrier. Assuming the total transmit power of all the antennas is normalized to be 1, then $C^{\mathrm{H}}C = M_{\mathrm{r}}$ and $W^{\mathrm{H}}W = M_{\mathrm{t}}$.

In order to evaluate the performance of MIMO-OFDM beamforming, the effective SNR is chosen as the criteria, which can be computed as,

$$\gamma_{\text{eff}} = -\beta \ln\left(\frac{1}{N}\sum_{m=1}^{N} \exp\left(-\frac{|C^H H_m W|^2}{\beta M_{\text{t}} M_{\text{r}} \sigma^2}\right)\right), \quad (13)$$

where $\beta$ is the system parameter depending on the coding rate. This equation is to map the vector SNR, which consists of the SNR on each subcarrier, to a scalar $\gamma_{\text{eff}}$, which will yield the same PER in an AWGN channel **[23]**.

For MIMO-OFDM systems, there are 3 beamforming schemes: subcarrier-wise beamforming, symbol-wise beamforming, and hybrid beamforming. The details about these three MIMO-OFDM beamforming schemes are discussed in the following part.

The block diagram of subcarrier-wise beamforming is shown in **Figure 10**. The block '$W_{m-1}$' and the block '$C_{m-1}$' are the weighting vector for the symbol on the *m*th subcarrier at transmitter and receiver respectively. In this beamforming system, each subcarrier has one SVD processor, which is shown as 'Beam Forming' in the block diagram. Moreover, one FFT/IFFT processor is required for each antenna.

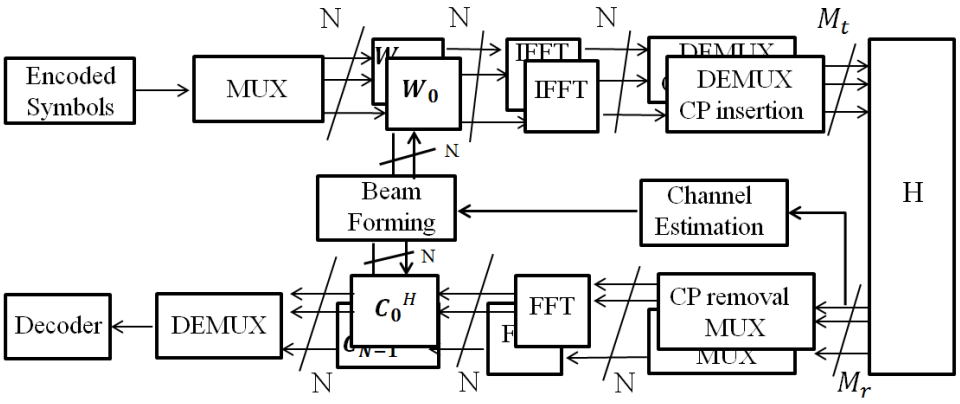


**Figure 10: Block diagram of subcarrier-wise beamforming**

With this beamforming scheme, the effective SNR in ( 13 ) becomes as,

$$\gamma_{\text{eff,subcarrier}} = -\beta \ln\left(\frac{1}{N}\sum_{m=1}^{N} \exp\left(-\frac{\max_{c,w}\left|C_m{}^{\text{H}} H_m W_m\right|^2}{\beta M_{\text{t}} M_{\text{r}} \sigma^2}\right)\right). \quad (14)$$

The maximization in ( 14 ) is to achieve the largest singular value of each $H_m$ through the operation $C_m{}^{\text{H}} H_m W_m$. In this way, $C_m$ is the first column of matrix $U_m$ and $W_m$ is the first column of matrix $V_m$. The bandwidth for 60 GHz communication is very large and the channel is

commonly frequency selective. This kind of beamforming can find the best weighting vectors for different subcarriers, so this technique is optimal. However, due to the hardware complexity, subcarrier-wise beamforming is not practical.

The hardware complexity can be reduced by using the other two beamforming schemes. The first one is symbol-wise beamforming shown in **Figure 11**. The same weighting vector is applied on all the subcarriers and only one IFFT/FFT processor is required at each terminal.

In addition, to avoid intensive computations, a set of pre-defined codebook **[24]** is used for weighting vector selection. For a 1-D phased array antenna with M radiating elements and K beams, the codebook matrix is given as,

$$W(m,k) = \mathrm{j}^{\mathrm{floor}\left(\frac{m*\mathrm{mod}\left(k+\left(\frac{K}{2}\right),K\right)}{K/4}\right)} \qquad (15)$$

$$m = 0 \ldots M-1; \quad k = 0 \ldots K-1$$

The column vectors **C** and **W** in **Figure 11** are chosen from the codebook matrix above.

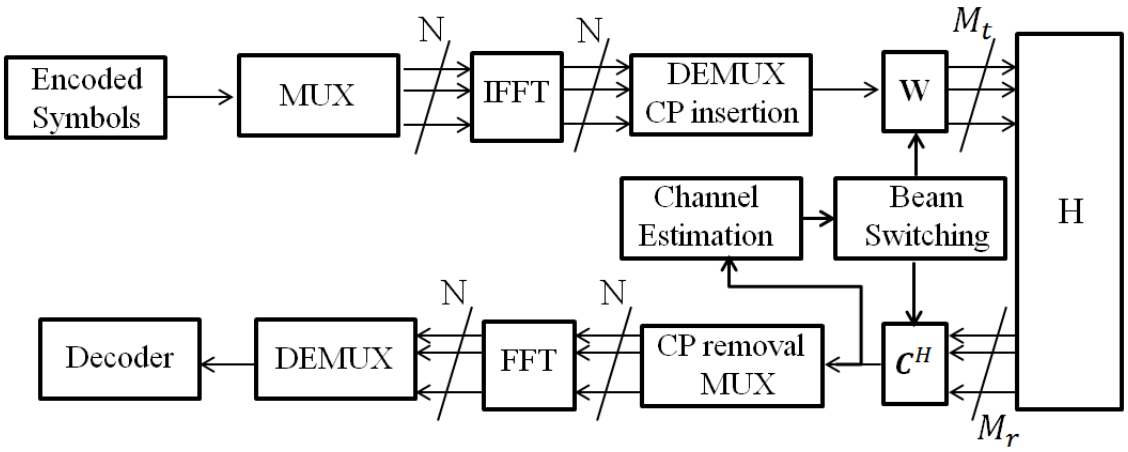


**Figure 11: Block diagram of symbol-wise beamforming**

The problem of symbol-wise beamforming is to find the best vector pair from the codebook to maximize the effective SNR,

$$\gamma_{\mathrm{eff,symbol}} = \max_{c,w \epsilon C} \left\{ -\beta \ln \left( \frac{1}{N} \sum_{m=1}^{N} \exp\left(-\frac{|C^{\mathrm{H}} H_m W|^2}{\beta M_{\mathrm{t}} M_{\mathrm{r}} \sigma^2}\right) \right) \right\}. \qquad (16)$$

However, as the symbol-wise beamforming just maximizes the effective SNR overall subcarriers, this leads to performance loss. As a result, **[26]** proposes a hybrid beamforming technique and makes combination of the two beamforming techniques mentioned before. The block diagram

for the hybrid beamforming technique is shown in **Figure 12**. As can be seen, the symbol-wise beamforming is applied at the transmitter side, while subcarrier-wise beamforming is employed at the receiver side. The beam codebook is also applied at the transmitter side. The effective SNR for this beamforming scheme can be computed as,

$$\gamma_{\text{eff,hybrid}} = \max_{w \epsilon C} \left\{ -\beta \ln \left( \frac{1}{N} \sum_{m=1}^{N} \exp\left( -\frac{\left| {C_{m,\text{opt}}}^{\text{H}} H_m W \right|^2}{\beta M_{\text{t}} M_{\text{r}} \sigma^2} \right) \right) \right\}, \quad (17)$$

where $C_{m,\text{opt}}$ is optimal shaping vector depending on the selected beam steering $W$ and $H_m$. According to Cauchy-Schwarz inequality theorem, $C_{m,\text{opt}}$ is given by,

$${C_{m,\text{opt}}}^{\text{H}} = \sqrt{M_{\text{t}}} \frac{W^{\text{H}} {H_m}^{\text{H}}}{\left\| W^{\text{H}} {H_m}^{\text{H}} \right\|}. \quad (18)$$

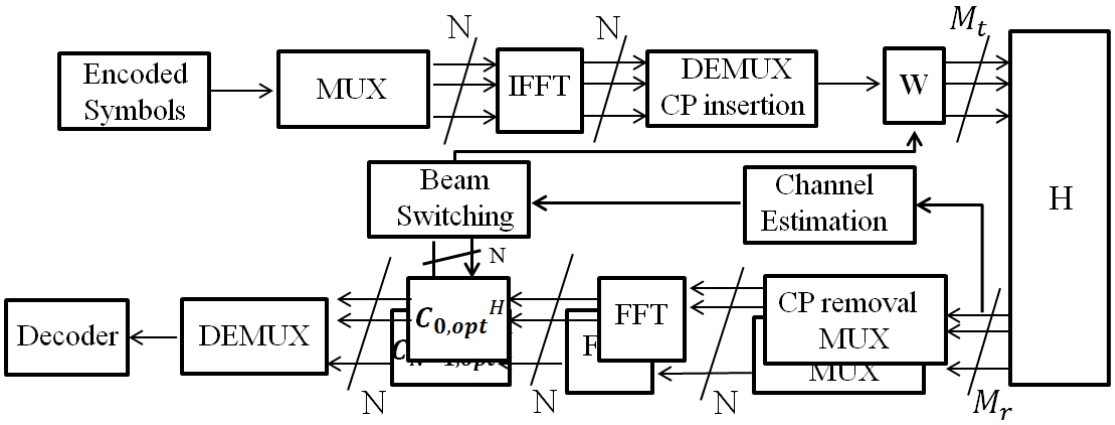


**Figure 12: Block diagram of hybrid beamforming**

## 3.2.2 Simulations

The simulation for the performance analysis of the above three MIMO-OFDM beamforming schemes is done in MATLAB.

### 3.2.2.1 Assumption

The channel model is generated at channel 2 of the unlicensed 60 GHz band (59.4 GHz to 61.56 GHz). The transceiver distance is 5m. The transmit power to noise ratio is 0 dB. The number of subcarriers is 512. According to **[23]**, the effective exponential SNR parameter is $\beta = 2$ for QPSK. The simulation considers two basic antenna arrays: uniform linear array (ULA) and uniform circular array (UCA). The antenna elements are spaced by $\frac{\lambda}{2} = 2.5mm$. Both the Line Of Sight (LOS) and Non Line Of Sight (NLOS) cases are considered. The channel estimation is

assumed perfect in this simulation. The number of antennas at the transmit side and the receive side are the same, i.e., $M_{\mathrm{r}} = M_{\mathrm{t}}$. Moreover, this simulation assumes the number of beam patterns is the same as the number of antenna elements ($M_{\mathrm{r}} = M_{\mathrm{t}} = K$) when generating the codebook.The antenna gain is assumed to be 0 dBi. Furthermore, the Doppler shift is assumed to be negligible, as transmitter and receiver are moving slowly relatively to each other.

### 3.2.2.2 Channel Model

The channel model used in this thesis is based on the one developed by IEEE 802.15.3c Task Group **[25]**. The impulse responses of the MIMO channel for ULA and UCA are given by ( 19 ) and ( 20 ) respectively.

$$h_{m,n}(t) = a_0\delta(t)\Phi_{m,n}({\theta^a}_0, {\theta^d}_0) + \sum_{l=1}^{L} a_l\delta(t-\tau_l)\Phi_{m,n}({\theta^a}_l, {\theta^d}_l)\,, \tag{19}$$

$$h_{m,n}(t) = a_0\delta(t)\Phi_{m,n}\left({\theta^a}_0, {\varphi^a}_0, {\theta^d}_0, {\varphi^d}_0\right) + \sum_{l=1}^{L} a_l\delta(t-\tau_l)\Phi_{m,n}({\theta^a}_l, {\varphi^a}_l, {\theta^d}_l, {\varphi^d}_l)\,, \tag{20}$$

where *m* refers to *m*th transmit antenna, *n* refers to *n*th receive antenna, $a_l$ is the amplitude of *l*th path and $\tau_l$ is the time delay of the *l*th path. These parameters are random variables, which are determined by specific environment. However, as mentioned in Section **3.1.2**, 60 GHz channel model for vehicles is missing. In this part, $a_l$ is assumed to follow Rayleigh distribution in NLOS channel and Rician distribution with K factor of 10 dB in LOS channel.

$\Phi_{m,n}({\theta^a}_l, {\theta^d}_l)$ is the steering matrix for $l$-th path depending on the Angle of Arrival ${\theta^a}_l$ (AoA) and Angle of Departure ${\theta^d}_l$ (AoD). It is computed as,

$$\Phi_{m,n}({\theta^a}_l, {\theta^d}_l) = \exp\left(\frac{\mathrm{j}2\pi(m-1)d\sin({\theta^a}_l)}{\lambda}\right)\exp\left(\frac{\mathrm{j}2\pi(m-1)d\sin({\theta^d}_l)}{\lambda}\right), \tag{21}$$

where $d$ is the space between antenna elements and ${\theta^a}_l$, ${\theta^d}_l$ are i.i.d. random values uniformly distributed over $\mathrm{U}[0, 2\pi)$.

$\Phi_{m,n}({\theta^a}_l, {\varphi^a}_l, {\theta^d}_l, {\varphi^d}_l)$ is the elements in the steering matrix for the $l$th path depending on the elevation angle of Arrival ${\theta^a}_l$, the azimuth Angle of Arrival ${\varphi^a}_l$, the elevation Angle of Departure ${\theta^d}_l$ and the azimuth Angle of Departure ${\varphi^d}_l$. It can be expressed as,

$$\Phi_{m,n}\left({\theta^a}_l, {\varphi^a}_l, {\theta^d}_l, {\varphi^d}_l\right) = \exp\left(\frac{\mathrm{j}2\pi r\sin({\theta^a}_l)\cos({\varphi^a}_l - \varphi_m)}{\lambda}\right)\exp\left(\frac{\mathrm{j}2\pi r\sin({\theta^d}_l)\cos({\varphi^d}_l - \varphi_m)}{\lambda}\right), \tag{22}$$

where $r$ ($r = \frac{d}{2\sin(\frac{\pi}{M_t})}$) is the radius of the circular array, ${\theta^a}_l$ and ${\theta^d}_l$ are i.i.d. random values uniformly distributed over $\mathrm{U}[0, \pi)$, and ${\varphi^a}_l$ and ${\varphi^d}_l$ are i.i.d. random values uniformly distributed over $\mathrm{U}[0, 2\pi)$.

### 3.2.2.3 Numerical results

The beamforming performance is evaluated by the beamforming gain, which is computed as,

$$\mathrm{G}_{\mathrm{beamforming}} = \frac{\gamma_{\mathrm{eff,beamforming}}}{\gamma_{\mathrm{eff,SISO}}}. \qquad (23)$$

**Figure 13** shows the beamforming gain of the three different schemes together with an upper bound in the LOS channel. The bound is the beamforming gain achieved when the MIMO channel is totally correlated in a special situation where all the antenna elements are placed in one single point and only one single path exists between the transmitter and the receiver. According to **[26]**, the bound can be calculated as,

$$\mathrm{G}_{\mathrm{bound}}[\mathrm{dB}] = 10\log_{10}(M_t M_r). \qquad (24)$$

It can be seen easily that because of the existence of LOS component, the performance of the three beamforming schemes don't have big differences. The more antennas are used, the higher gain can be obtained.

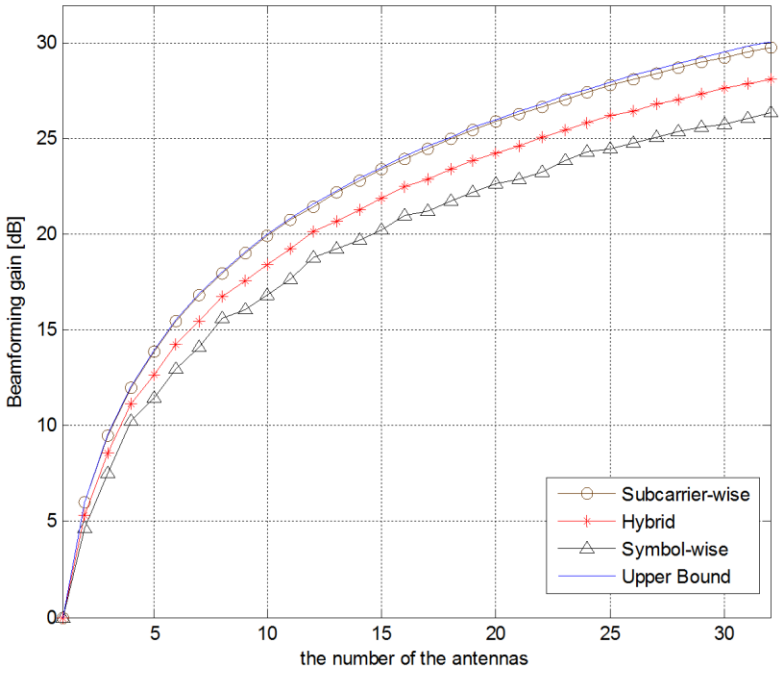


**Figure 13: Beamforming gain as a function of the number of antennas (ULA) in LOS channel**

On the contrary, when no LOS component exists, the performance of the beamforming degrades (shown in **Figure 14**). The reason is that the environment is rich-scattering and the channels of different links are less correlated. The performance differences are also visible in **Figure 14**. The subcarrier-wise beamforming is the best, followed by the hybrid scheme and the symbol-wise beamforming is the worst. For the subcarrier-wise scheme and the hybrid scheme, more antennas lead to higher gain. However, this improvement degrades with the growth in the number of antennas. For symbol-wise beamforming, there is no obvious improvement from antenna increment when the number of antenna elements reaches to a certain value. This value depends on the propagation environment, antenna gain and the Doppler shift.

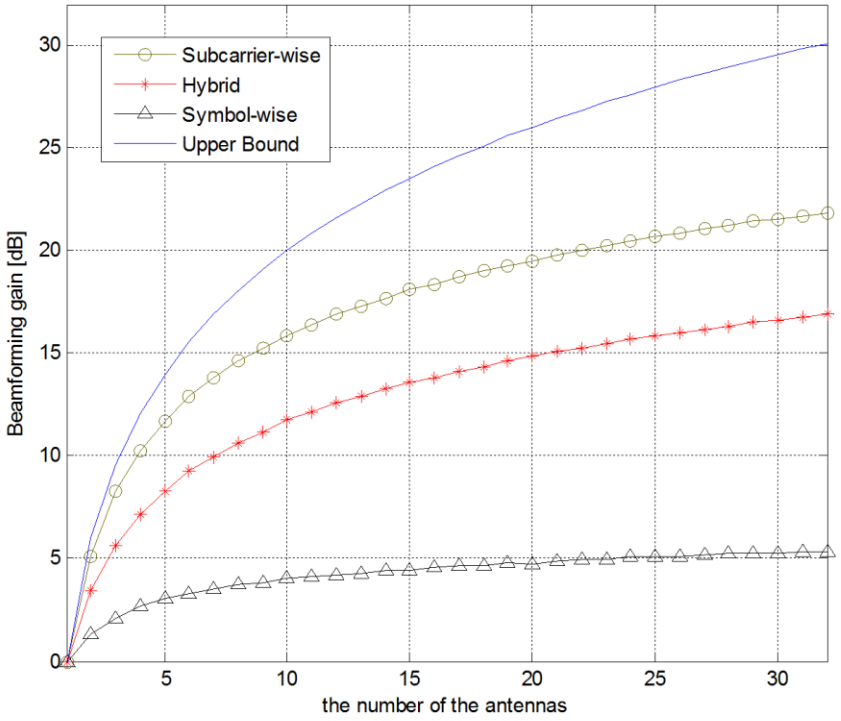


**Figure 14: Beamforming gain as a function of the number of antennas (ULA) in NLOS channel**

**Figure 15** and **Figure 16** show that with UCA, the beamforming gains have similar trends as those of ULA. But in LOS channel, the performance differences among these three schemes are more obvious. The reason is that the codebook in the standard is designed for 1-D phased array antennas or 2-D phased rectangular grid antennas. In other words, this codebook is not very suitable for circular array antennas.

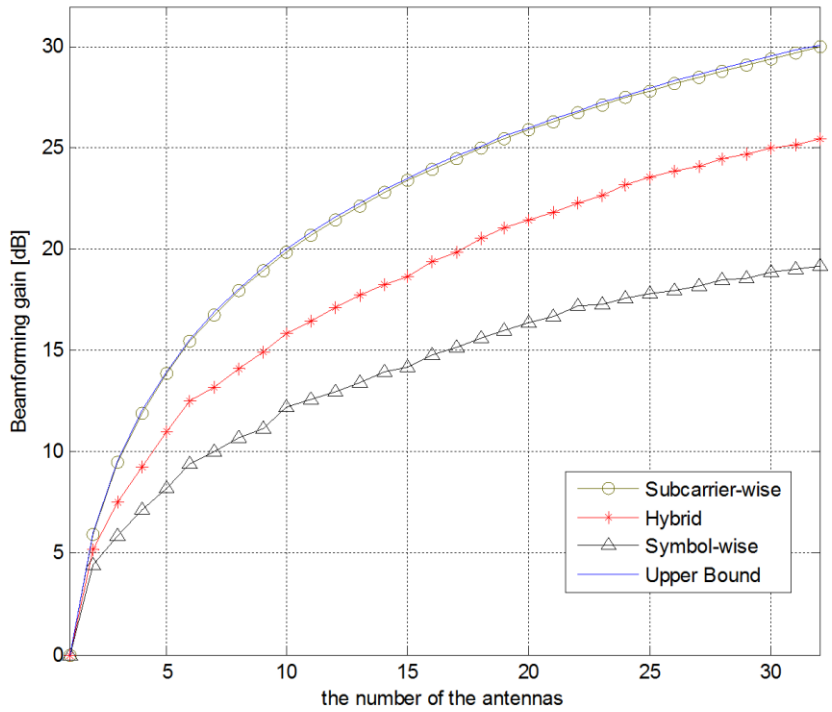


**Figure 15: Beamforming gain as a function of the number of antennas (UCA) in LOS channel**

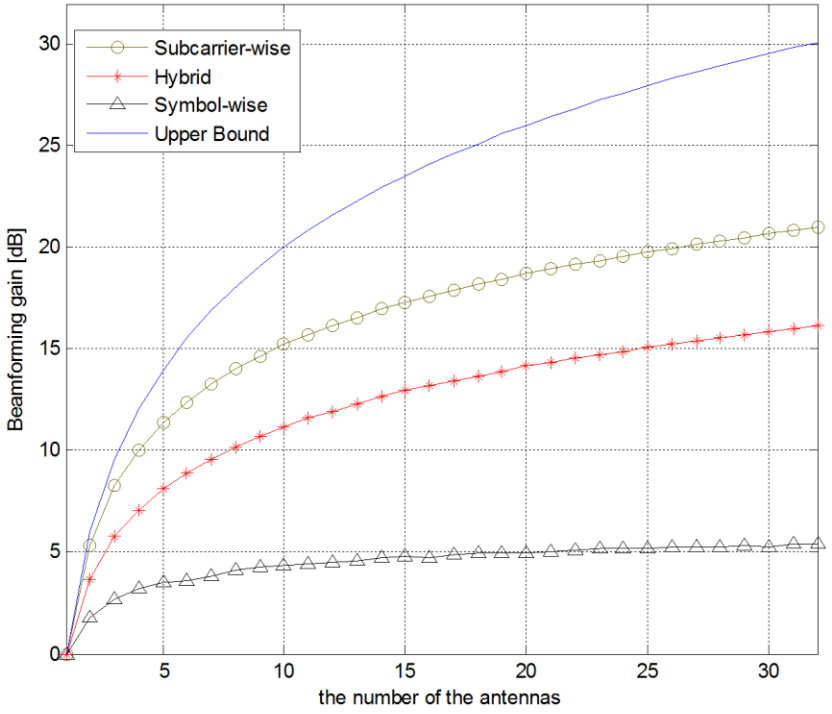


**Figure 16: Beamforming gain as a function of the number of antennas (UCA) in NLOS channel**

# Chapter 4

# Test in vehicle

This chapter mainly presents the test environment and the measurement results. A detailed description of the test plan can be found in **Appendix A.**

## 4.1 Definition

### 4.1.1 Problem statement

In Chapter 3, the theoretical analysis is performed to evaluate the link range and beamforming performance of the standard IEEE 802.11ad. However, the mathematical models available are often generalized for non-vehicular environment and cannot cover all the factors in practice, especially in vehicle communications. Therefore, the test in a real vehicle is necessary to get better knowledge of practical situation.

### 4.1.2 Test scope

The test focuses on the communication performance on the physical layer and data link layer of a wireless link. The targets of this test are to evaluate whether reliable high throughput communication can be achieved in the following situations:

- The communication operated inside the vehicle, in the region of passenger compartment;
- The communication operated between vehicle and outside service point;
- The communication distance in outdoor channel up to 10 meters or farther.

## 4.2 Test environment

### 4.2.1 Test overview

The vehicle should be equipped with a transceiver supporting the IEEE 802.11ad standard. This transceiver shall connect to another transceiver, which is placed within the vehicle compartment on specific test positions. Besides, the vehicle transceiver shall also connect to the transceiver, which is located outside the car at a short range distance.

As shown in **Figure 17**, the test is conduct with laptops and the evaluation boards (EVBs) (shown in **Figure 18**), whose specifications are presented in **Table 4**. The connection between evaluation boards and laptops is achieved with USB 3.0 cable.

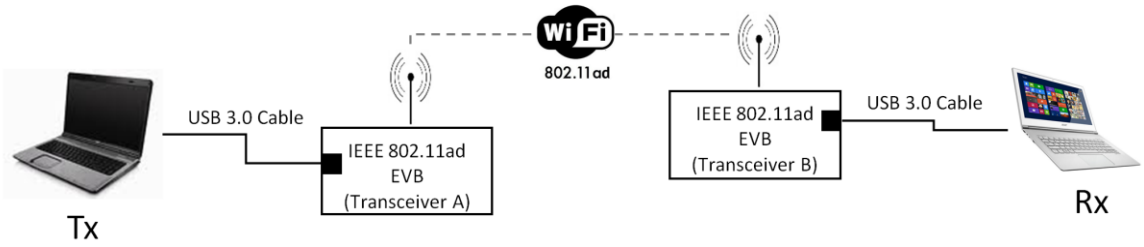


**Figure 17: Overview of test using evaluation boards**

**Figure 18: The evaluation board used for the test**

**Table 4: The specifications of the evaluation boards**

| | |
|---|---|
| Radio | 2 × 2 MIMO with beamforming |
| Antenna type | Horizontally polarized |
| Antenna coverage angle | +/- 30 degree horizontally, +/- 60 degree vertically |
| EIRP | 12.5 dBm |
| Noise figure (Rx) | 7.5 dB |
| Implementation Loss (Rx) | 7.5 dB |
| Communication Bandwidth | 1.76 GHz |
| Antenna gain with beamforming | 7.5 dBi |
| Clock frequency | 100 MHz |
| MCS (supported) | 0~7 |

### 4.2.2 Test scenarios & test positions

The test is conduct in the following three scenarios:

Scenario 1 This scenario refers to the communication inside the vehicle. Both the transmitter and the receiver are located inside the vehicle (shown in **Figure 19**). The red points denote the specific test positions of **transceiver A** which represents the WLAN hot spot inside the vehicle. The blue points denote the specific test positions of **transceiver B**, which represents the application terminals.

Scenario 2 This scenario also refers to the communication inside the vehicle, but focuses more on the possible situation of the communication between the ECUs at certain positions. As shown in **Figure 20**, the red points denote the test positions of **transceiver A** (the wireless communication interface of one ECU), and the blue points denote the test positions of **transceiver B** (the wireless communication interface of another ECU).

Scenario 3 This scenario refers to the communication between the vehicle and the service infrastructure. **Transceiver A** is located at a platform outside the vehicle with a specific height from the ground (see **Figure 21**). It represents the WLAN hot spot at service infrastructure. **Transceiver B** is placed at two different positions: the external roof of the vehicle and the position under the rear view mirror inside the vehicle. The comparison of the performance at these two different positions is helpful to reflect the effect of vehicle body on the 60 GHz signal.


**Figure 19: Test positions in Scenario 1 (Source: [27]), red points denote test positions of transceiver A, and blue points denote test positions of transceiver B**


**Figure 20: Test positions in Scenario 2 (Source: [27]), red points denote test positions of transceiver A, and blue points denote test positions of transceiver B**


**Figure 21: Test positions in Scenario 3 (Source: [27]), red points denote test positions of transceiver A, and blue points denote test positions of transceiver B**

### 4.2.3 Environment setup

The default configuration for the test is shown in **Table 5**.

**Table 5: The default configuration of the test**

| | |
|---|---|
| Test vehicle | The new Volvo XC 90 D5 |
| Passengers | One driver, one passenger on the rear left seat |
| Indoor Temperature | 20.5 $^0$C at front seat, 22.5 $^0$C at rear seat |
| Outdoor weather | Sunny, 14 $^0$C |
| Vehicle condition | Stand still but the engine on |

In **Scenario 1** and **Scenario 2**, **transceiver A** is placed at three different positions as visible in **Figure 22**. **Transceiver B** is located at different positions as shown in **Figure 23**.

(a) EVB placed on the central speaker [red 1].

(b) EVB placed next to the rear view mirror [red 2].

(c) EVB placed on the rear ceiling [red 3].

**Figure 22: Photographs of transceiver A taken during measurement phase**

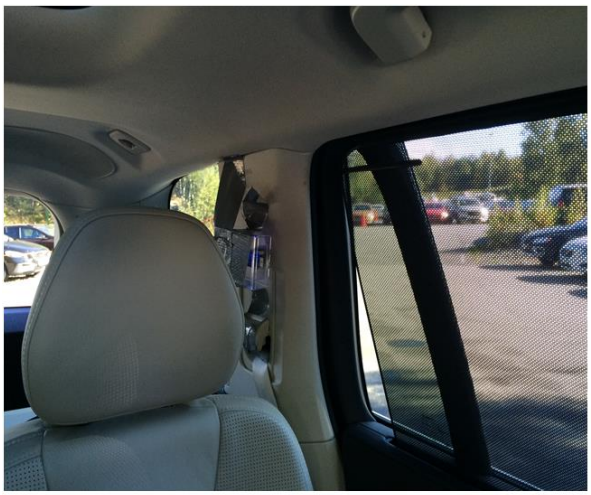

(a) EVB placed on the left IC bone [blue 9].

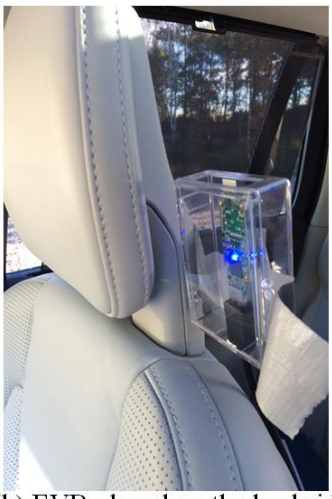

(b) EVB placed on the backside of front right headrest [blue 3].


(c) EVB placed on the central screen [blue 1].

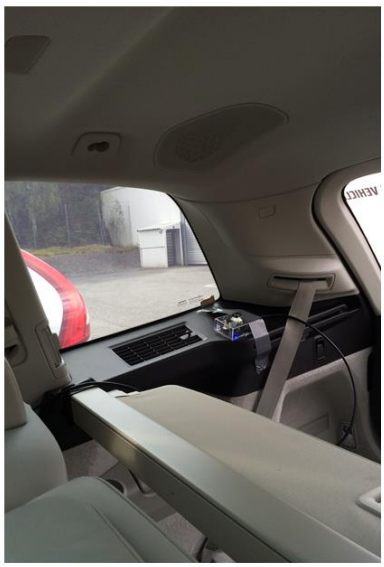

(d) EVB placed on the rear right trunk [blue 7].

**Figure 23: Photographs of transceiver B taken during test phase**

For **Scenario 3**, **transceiver A** is placed on the platform (fire stairs) at the height of 2 meters from the ground, as visible in **Figure 25**. The photographs of **transceiver B** are shown in **Figure 24**.

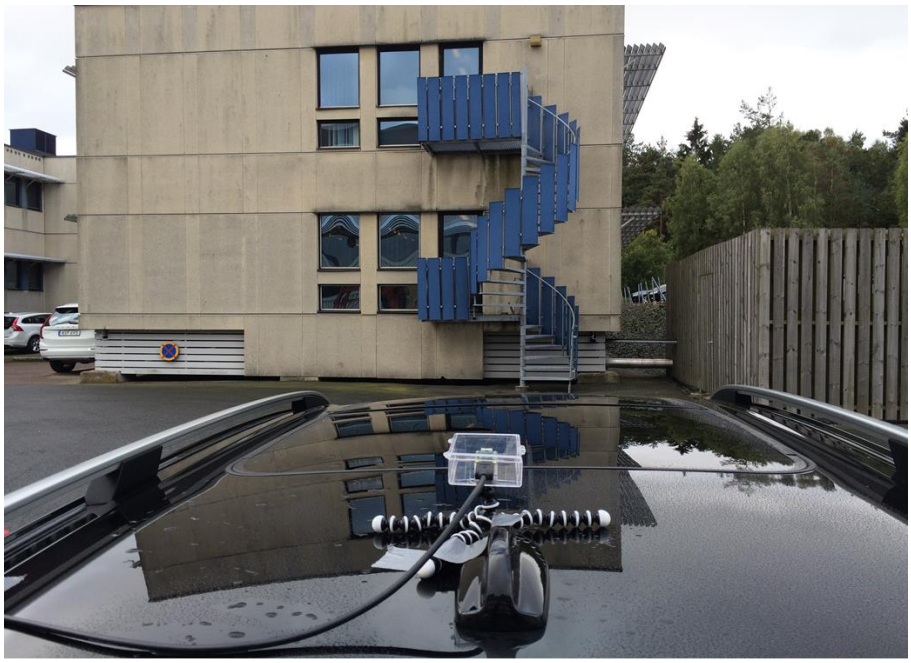

(a) EVB placed on the external roof [red 4].

(b) EVB placed under rear view mirror [red 5].

**Figure 24: Photographs of transceiver B taken in test scenario 3**

**Figure 25: Photographs of transceiver A (yellow circle) taken in the test Scenario 3**

## 4.3 Data collection

### 4.3.1 Key data collected

Because of different purposes listed in **Table 6**, in test stage the following key parameters are collected by the software. The packet size is 4096 bytes. The data of these parameters is refreshed and logged into the file every 100 milliseconds.

- **Effective data throughput**: the average number of bits of information data transferred per second from TX and accepted by RX. In this project, it's the average bitrate during the period of 100 milliseconds. It's measured after the MAC layer processing, which is a sublayer of the data link layer in OSI model. It describes the data throughput of MAC Service Data Unit (MSDU). The overhead on MAC layer leads to the decrease in effective throughput from PHY layer to MAC layer. Similarly, the overhead on PHY layer makes the effective throughput on PHY layer smaller than raw data rates, which are shown in **Table 3**.
- **Packet Error Rate (PER):** the number of packets received with Frame Check Sequence (FCS) error over the total number of received packets on the MAC layer. The evaluation kit doesn't have error correction algorithms, so the system just retransmits the packets when the errors are detected. The collected data of PER is calculated after the retransmission.

- **Received Channel Power Indicator (RCPI)**: the measurement of received RF power in the selected channel over the current frame at the time instance of data collection. It's measured on the physical layer.

**Table 6: The purposes of the collected data**

| Collected Data | Purpose |
|---|---|
| Effective data throughput (Mbps) | Measure the transmission capacity |
| Packet Error Rate (%) | Evaluate the communication quality |
| RCPI (dBm) | Analyze the path loss between TX and RX |

### 4.3.2 Pre-analysis of causes on bad performance in test

During each measurement, the performance may be affected by different factors. Some of them may cause serious degradation. It's thus important to have a pre-knowledge of them before performing the measurement. As visible in **Figure 26**, a parameter diagram (P-diagram) is created to analyze the factors that may affect the performance of desired ideal condition. In **Figure 26**, the control factors are the variants that can be controlled by the tester in the test, while the noise factors are the possible uncontrolled factors. This is a high level analysis. If we focus on the 'error states' in the P-diagram and digging into it, a Fishbone diagram shown in **Figure 27** can be created, which presents the possible causes grouped into 6 major categories, e.g. environment, man power, method, of the bad communication performance in the test. The Fishbone diagram together with P-diagram can provide some guidance when analyzing the measurement results in the test phase.

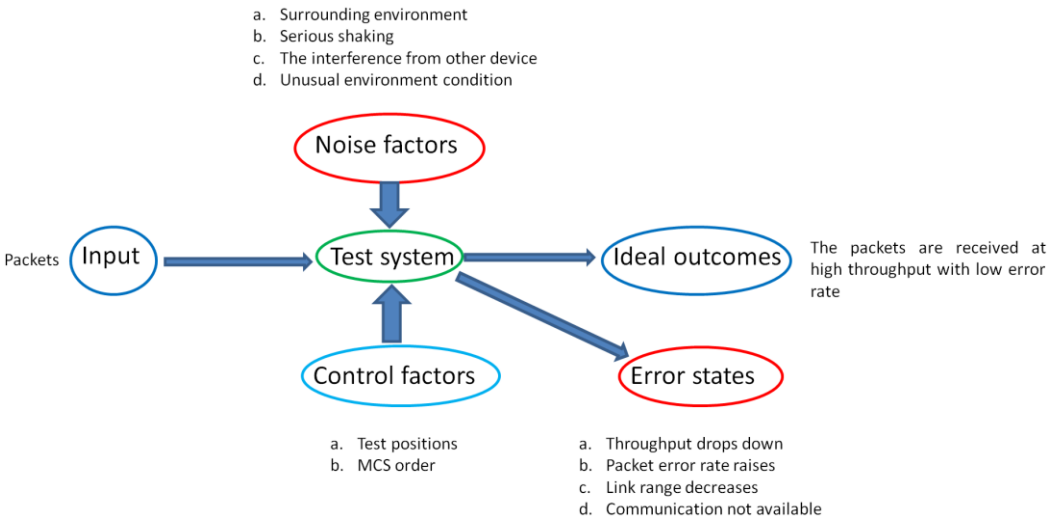


**Figure 26: P-diagram on the test measurement**

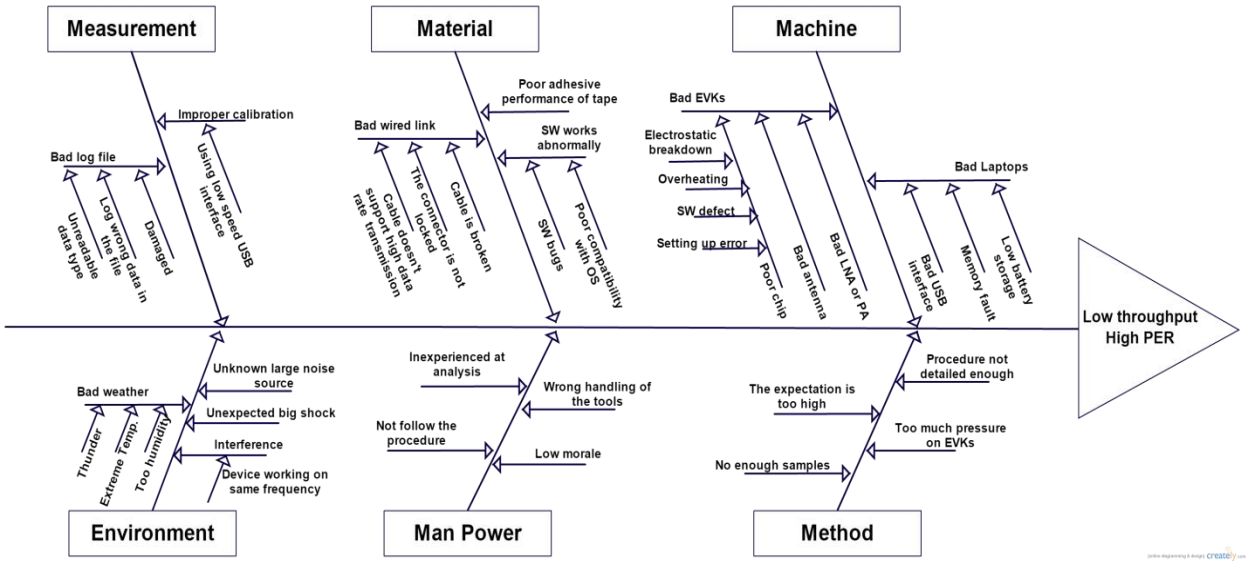


**Figure 27: Cause and effect (Fishbone) diagram on test measurement**

## 4.4 Test execution

The data collection is iterated for 5 times in all test cases. The duration of each time is 30 seconds

### 4.4.1 Test execution in Scenario 1 & 2

1. Set the test environment according to test configuration
2. Place evaluation board at one specific test position according to Section **4.2.2** and fix it
3. Connect the boards with the laptops
4. Start the software "Speedtest.exe"
5. Click the button "Connect" to connect the software with the evaluation boards
6. Change the MCS order to be 7
7. Click the button "Tx on" at transmitter side to start the transmission
8. Check whether the effective data throughput is beyond 120 Mbps for 8 seconds. If yes, move to step 9. If not, decrease the MCS order by 1 and repeat step 8
9. Log the data for 30 seconds and record the MCS order
10. Turn off the transmitter
11. Verify that the log file is created correctly and rename it with test ID and iteration No.
12. Repeat step 6 – 11 until all iterations are covered
13. Repeat step 2 – 12 until the measurement is performed in all test cases
14. Close the software and disconnect the evaluation boards
15. Collect and check all the materials

### 4.4.2 Test execution in Scenario 3

1. Set the test environment according to test configuration
2. Place evaluation board A on the outdoor platform
3. Place another evaluation board B at [red 4] and fix it at this position
4. Move the vehicle to the distance of 1 meter in front of the outdoor service point
5. Connect the boards with the laptops
6. Start the software "Speedtest.exe"
7. Click the button "Connect" to connect the software with the evaluation boards
8. Change the MCS order to be 7
9. Click the button "Tx on" at transmitter side to start the transmission
10. Check whether the effective data throughput is beyond 120 Mbps for 8 seconds. If yes, move to step 11. If not, decrease the MCS order by 1 and repeat step 10
11. Log the data for 30 seconds, and record the MCS order and the distance
12. Turn off the transmitter
13. Verify that the log file is created correctly and rename it with test ID and iteration No.
14. Repeat step 8 – 13 until all iterations are covered
15. Check whether the MCS order in all iterations is smaller than 1. If yes, skip to 17. Otherwise, continue.
16. Increase the distance between vehicle and outdoor service point by 1 meter and repeat step 8 – 15
17. Place another evaluation board B at [red 5] and fix it at this position
18. Repeat step 4 – 16
19. Close the software and disconnect the evaluation boards
20. Collect and check all the materials

### 4.4.3 6 sigma process of test execution

The 6 sigma process is a structured approach to drive the improvement in test process. It not only includes the flow chart of the whole test phase, but also brainstorms the possible output in practice after each step. Besides, during the analysis in this process, extra steps may be discovered and added to fix the possible output that fails to pass an initial inspection. The 6 sigma process mapping of the test in this project is shown in **Figure 28**.

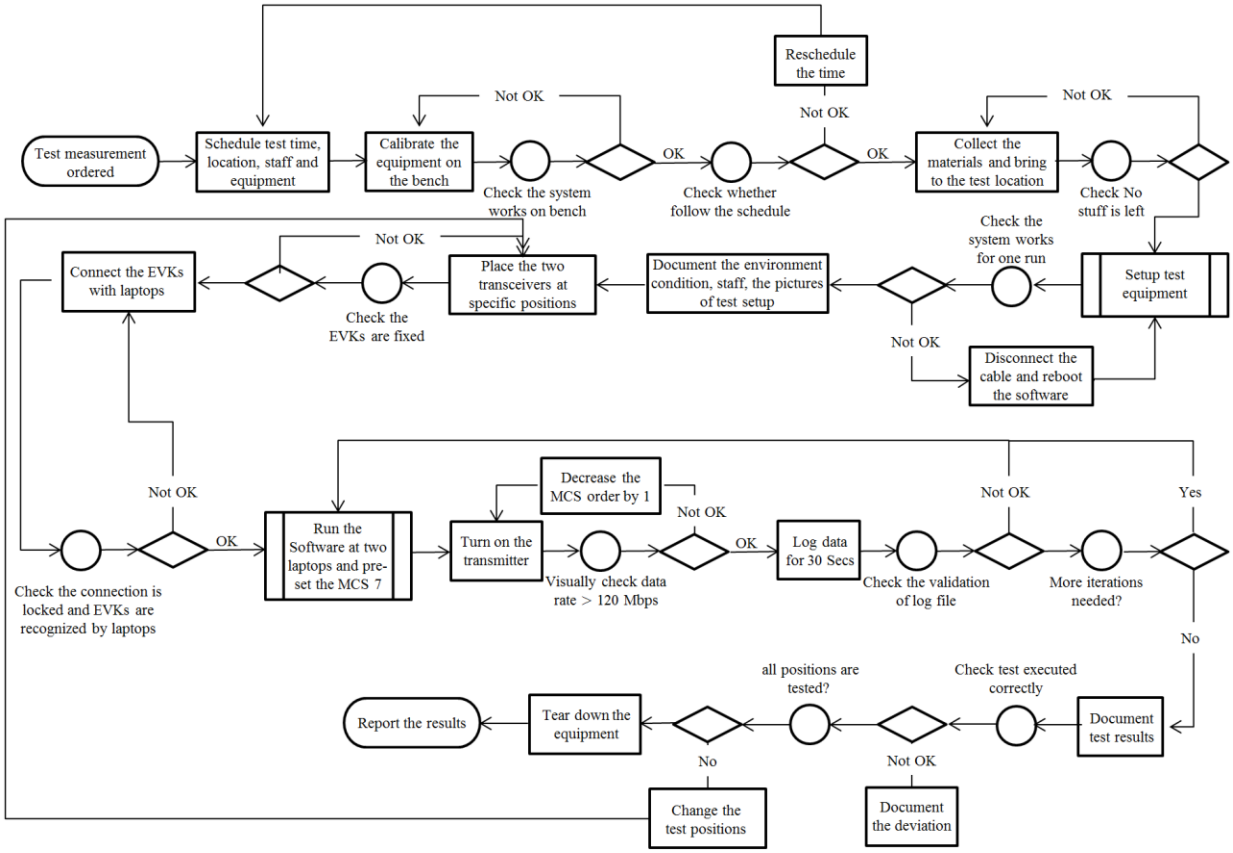


**Figure 28: 6 sigma process of test execution**

## 4.5 Results & analysis

### 4.5.1 Communication performance in test Scenario 1

The measurements in this scenario are performed under the default configuration, and two transceivers are placed at different positions defined in Section **4.2.2**.

As can be seen in **Figure 29**, when the WLAN hot spot (**transceiver A**) is placed at the position of the central speaker, the communication is available at all test positions except the rear left seat. However, the performance varies a lot at these positions. For instance, since the LOS path exists between central speaker and the backside of the front headrests, the performance at (blue 3) and (blue 4) shown in **Figure 19** is the best. The average MAC layer data throughput is over 800 Mbps with an average PER of 7%. While due to antenna's directionality and obstacles (e.g. seats), nearly no LOS path exists between central speaker and other positions such as central screen and rear seats, and thus only low throughput communication is achieved at these positions. The performance is the worst at the front right seat, because **transceiver B** is placed outside of **transceiver A**'s antenna coverage angle and in a different polarization plane. The average data

throughput is just 86.4 Mbps and with an average PER of 29%, which is unacceptable in practice.

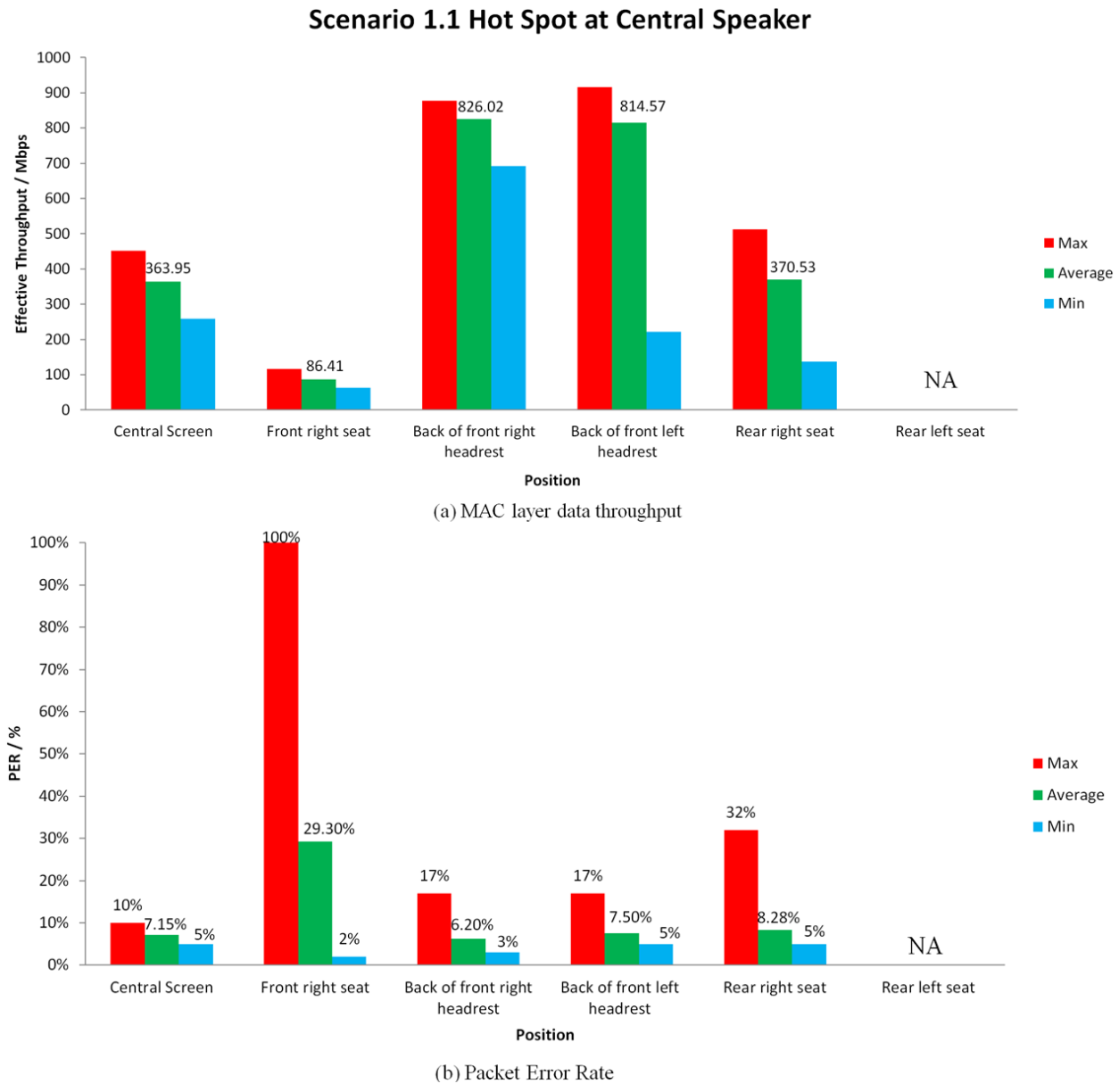


**Figure 29: Measured communication performance in Scenario 1.1**

As explained before, the performance is not good at 'Rear right seat' due to blocked LOS path by the front right seat. Furthermore, when the receiver is placed at 'Rear left seat', due to the existence of driver, in addition to the front seat human body is also the obstacle between transmitter and receiver. Therefore, the different results at 'Rear right seat' and 'Rear left seat' implies that human body also has big shadowing effect on signal transmission. A clearer view of this effect can be obtained when observing the results over the time samples at 'Back of the front

left headrest'. In this test case, as shown in **Figure 30**, we imitated some possible actions of driver: moving hands around the center console (during the purple color marked time period), operating the control buttons of skylight back and forth (during the red color marked time period). These actions led to the extreme changes in the communication performance. When the driver's body blocked the LOS path, the data throughput drops down, packet error rate rises up and nearly no signal is available at some time instant. In this situation these activities do not lead to a big problem due to the short duration. However, in practice high throughput communication may not be available at some specific positions inside the vehicle because of the serious shadowing effect of human body on 60 GHz signal.

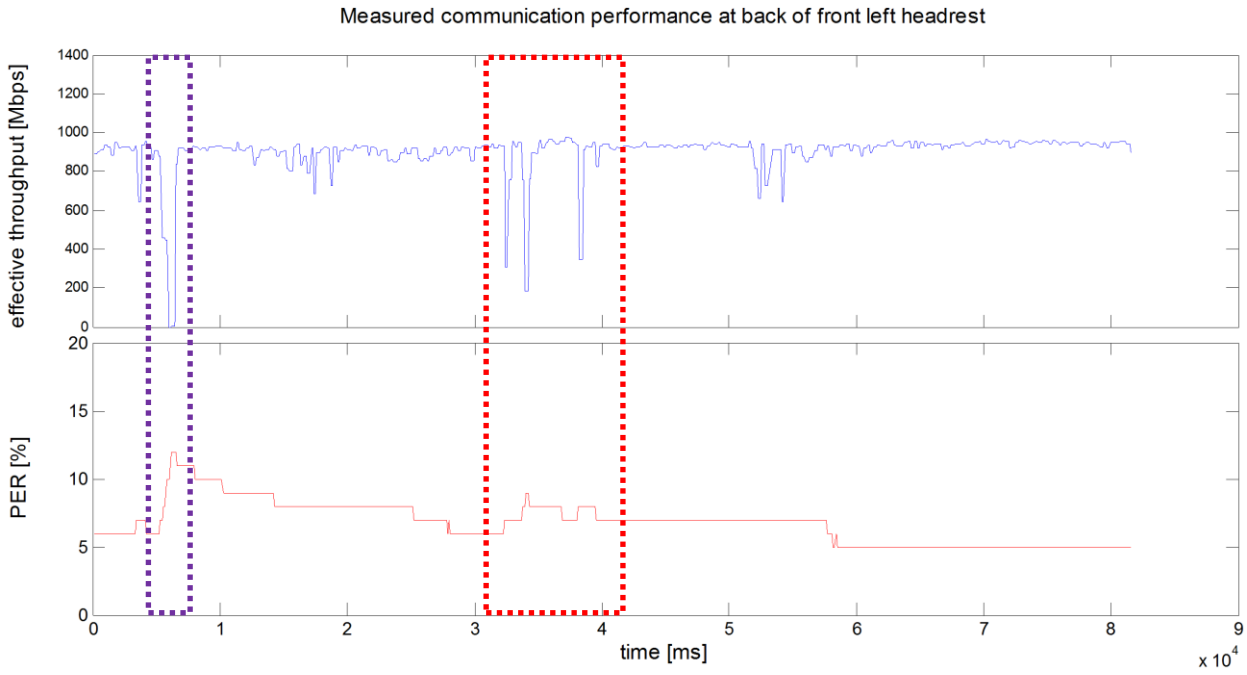


**Figure 30: Communication performance at back of front left headrest**

If the WLAN hot spot (**transceiver A**) is not placed at the central speaker, but next to the rear view mirror, it only covers the positions at the backside of the front headrests as visible in **Figure 31**. The main reason is that the vertical coverage angle of the antenna decreases to -30/+30 degree when **transceiver A** is placed as shown in **Figure 22b**. As a result, only the test positions at the backside of headrests are within **transceiver A**'s coverage angle. The performance at these positions is good with high data throughput and low packet error rate. However, because the driver's head was moved in front of transceiver A and blocked the LOS path, the large maximum value appears in the PER diagram, which indicates the big effect of human body again.

As can be seen in **Figure 32**, the position of the central main screen and the backside of the front headrests can be covered if the WLAN hot spot (**transceiver A**) is shifted to the rear ceiling

position. In general, the performance at these positions is fine, especially in terms of PER. But the data throughput varies obviously at different positions. The performance is best at the position 'Central screen', followed by the ones at the backside of the front headrests. From 'Central screen' to 'Back of front right headrest', the decrement in data throughput is because of the horizontal polarization of the antennas. When the orientations of the two transceivers are not in the same horizontal plane or two parallel horizontal planes, the transmission suffers more path loss, which may lead to the degradation in data throughput. The reason for the different performance in 'Back of front right headrest' and 'Back of front left headrest' is the shadowing effect of human body of the passenger sitting on the rear left seat.

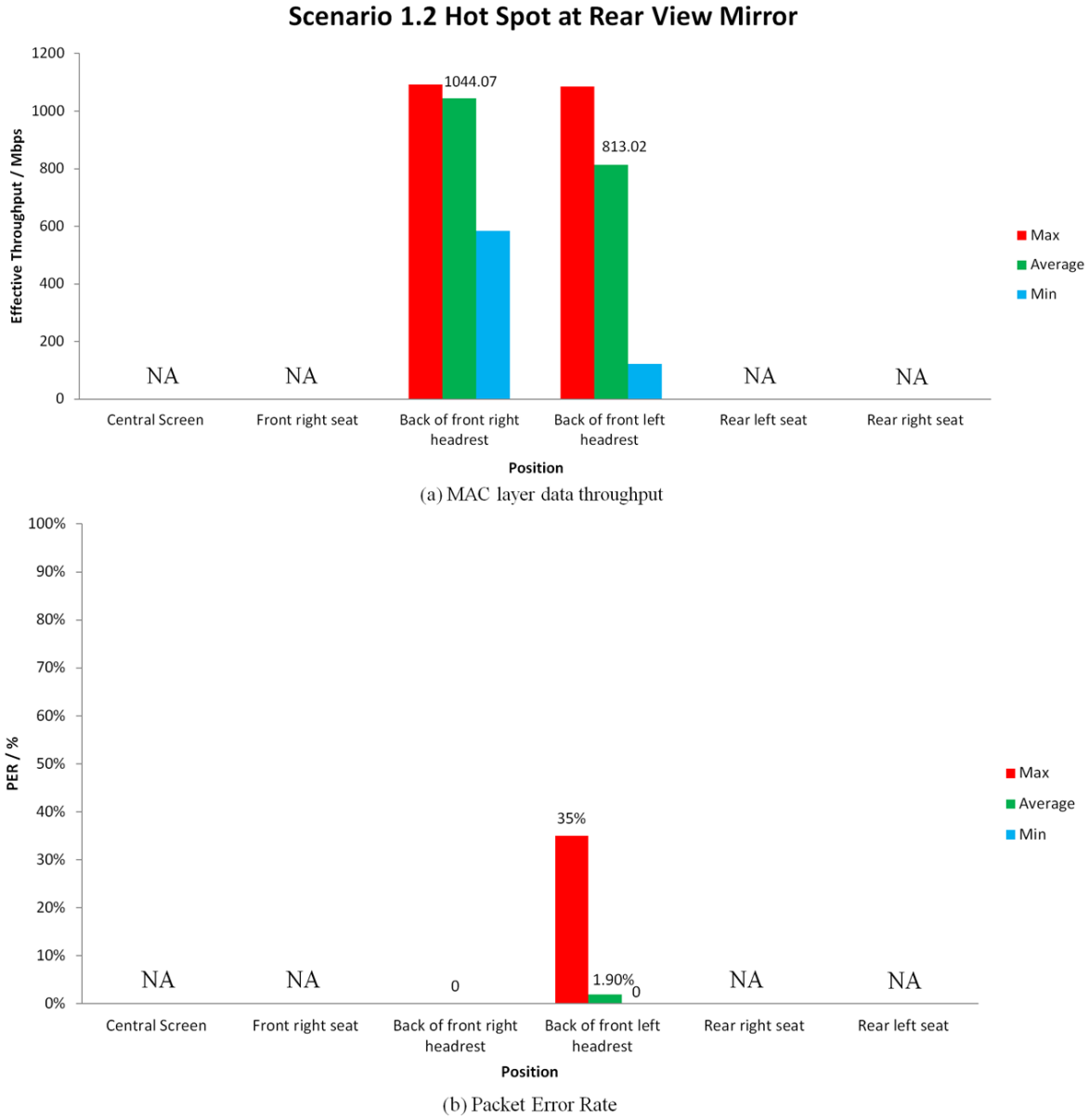


**Figure 31: Measured communication performance in Scenario 1.2**

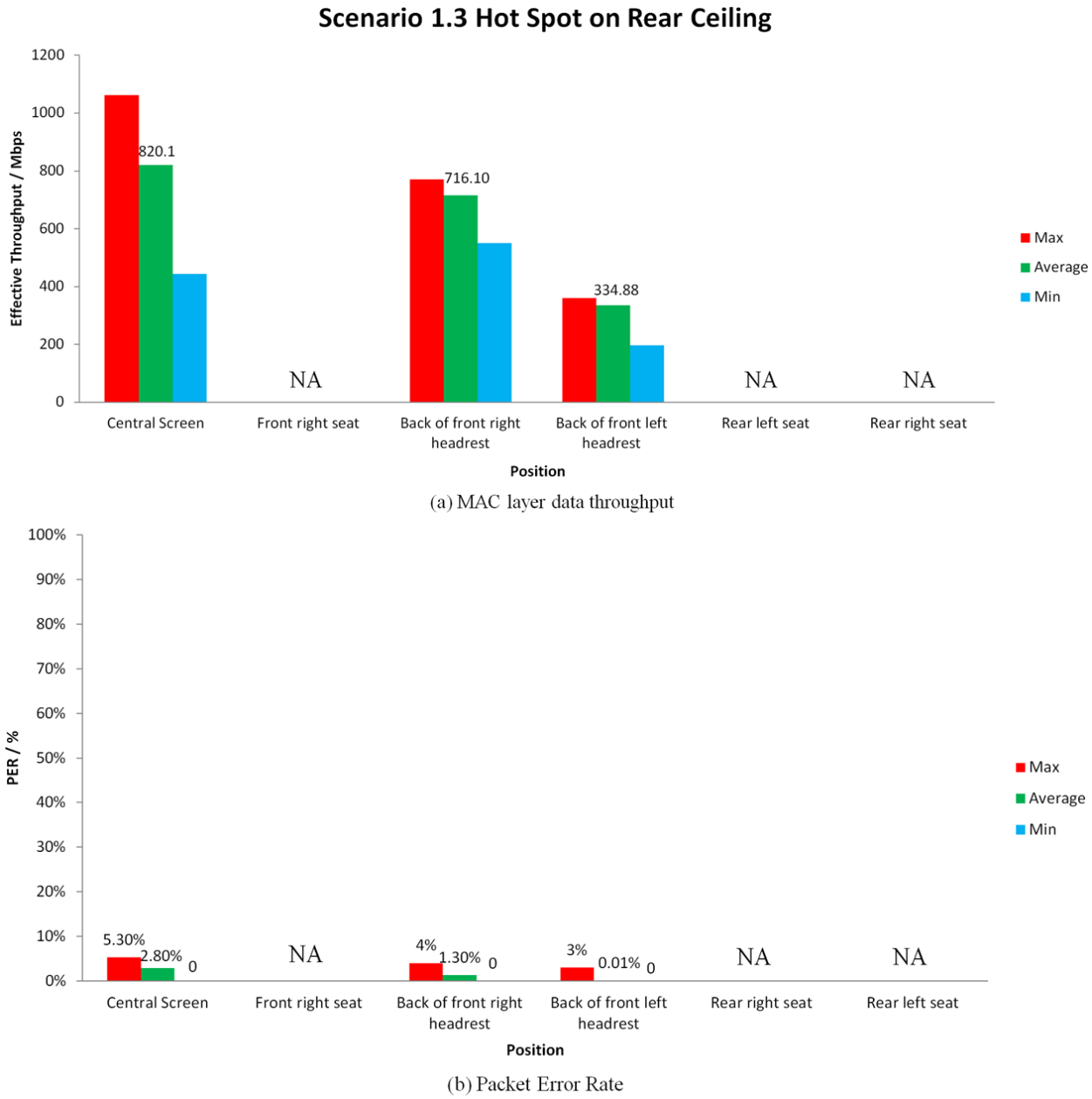


**Figure 32: Measured communication performance in Scenario 1.3**

## 4.5.2 Communication performance in test Scenario 2

As stated in Section **4.2.2**, in this scenario two transceivers are placed at different positions where ECUs are mainly installed. The performance of the point to point communication is measured under the default configuration. In general, according to the measurement results especially the PER diagram in **Figure 33**, the standard IEEE 802.11ad may be only feasible for

the communication between the ECUs near the central screen and the ECUs at the rear ceiling or the communication between the ECUs near the central speaker and the ECUs near the central screen. The poor performance in test cases '2', '3' and '9' is because of NLOS situations and the limitation of horizontal polarized antenna, which is already explained in Section **4.5.1**. The reason for the bad performance in '6' is the antenna's narrow coverage angle in the vertical plane in combination with the antenna's horizontal polarization. The different performance in '4' and '5' and the different performance in '7' and '8' is the result of the shadowing effect of human body.

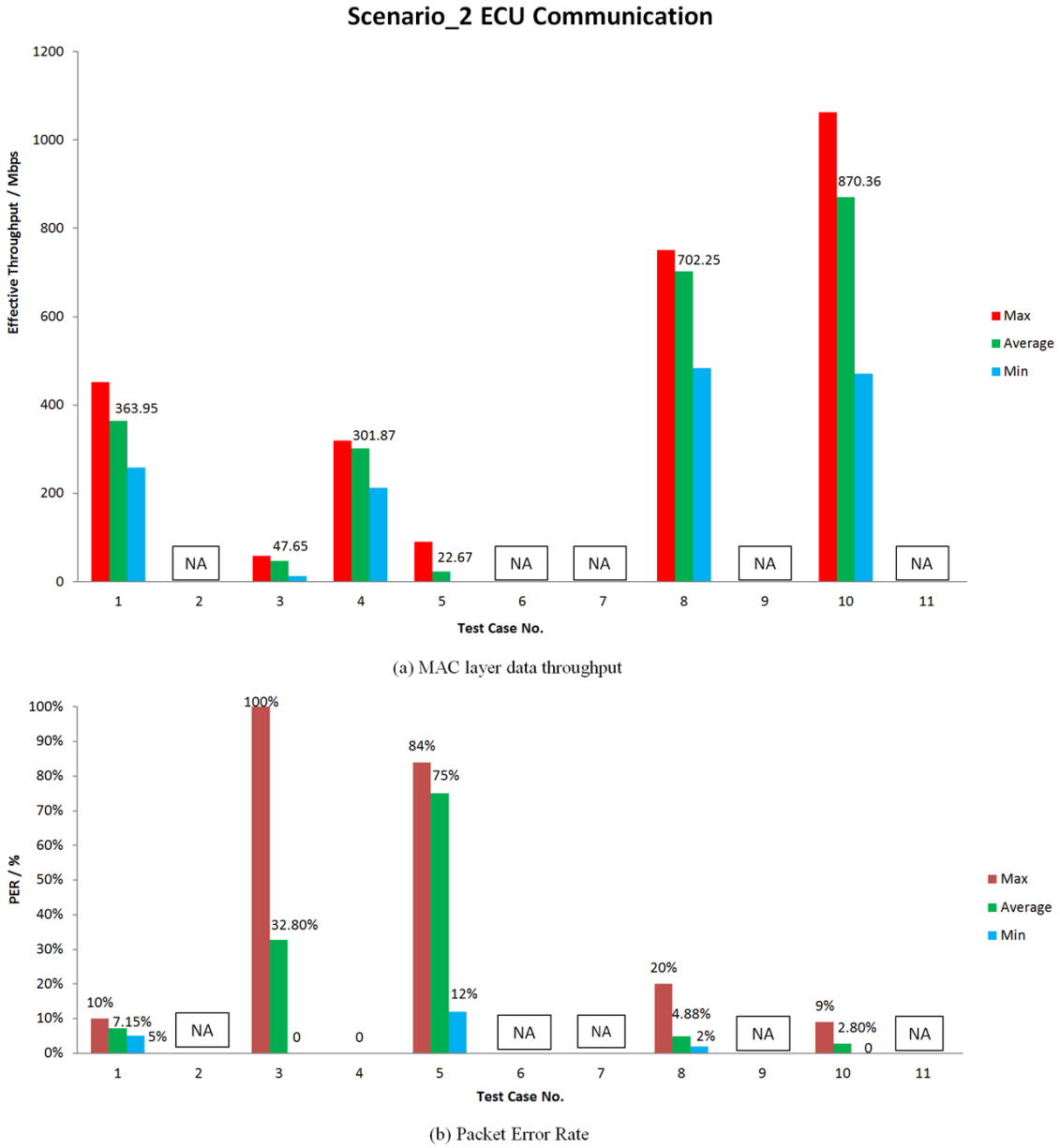


(a) MAC layer data throughput

(b) Packet Error Rate

**Figure 33: Measured communication performance in Scenario 2**
**(The description of different test case no. is shown in Table 7)**

**Table 7: Description of different test cases in Scenario 2**

| Test Case No. | Description |
|---|---|
| 1 | Communication between the ECUs at central speaker and central main screen |
| 2 | Communication between the ECUs at central speaker and left IC bone |
| 3 | Communication between the ECUs at central speaker and right IC bone |
| 4 | Communication between the ECUs at central speaker and rear right trunk |
| 5 | Communication between the ECUs at central speaker and rear right trunk but with passenger on rear right seat |
| 6 | Communication between the ECUs at rear view mirror and central main screen |
| 7 | Communication between the ECUs at rear view mirror and left IC bone |
| 8 | Communication between the ECUs at rear view mirror and right IC bone |
| 9 | Communication between the ECUs at rear view mirror and rear right trunk |
| 10 | Communication between the ECUs at central main screen and rear ceiling |
| 11 | Communication between the ECUs at central main screen and rear right trunk |

### 4.5.3 Path loss parameters estimation

In this part, the path loss parameters are estimated for the model ( 2 ). The measured data set can be modeled as **[28]**,

$$\boldsymbol{y} = \boldsymbol{X}\boldsymbol{\alpha} + \boldsymbol{\epsilon}\,, \qquad (25)$$

where

$$\boldsymbol{y} = \begin{pmatrix} P_{\mathrm{L}}(d_1) \\ P_{\mathrm{L}}(d_2) \\ \vdots \\ P_{\mathrm{L}}(d_K) \end{pmatrix}, \boldsymbol{X} = \begin{pmatrix} 1 & 10\log_{10} d_1 \\ 1 & 10\log_{10} d_2 \\ \vdots & \vdots \\ 1 & 10\log_{10} d_K \end{pmatrix}, \boldsymbol{\epsilon} = \begin{pmatrix} \epsilon_1 \\ \epsilon_2 \\ \vdots \\ \epsilon_K \end{pmatrix} \text{ and } \boldsymbol{\alpha} = \begin{pmatrix} P_{\mathrm{L}}(d_0) \\ \mathrm{n} \end{pmatrix}$$

The vector $\boldsymbol{y}$ is the data set of the path loss, which is calculated as ( 26 ) based on the measured **RCPI**.

$$y_i = \mathrm{EIRP} - (\mathrm{RCPI}_i - G_{\mathrm{r}} + \mathrm{IL})\,, \qquad (26)$$

where EIRP is 12.5 dBm, $G_r$ is 7.5 dBi and implementation loss (IL) is 7.5 dB according to **Table 4**.

By applying the ordinary least squares (OLS) mentioned in **[28]**, the parameter vector $\boldsymbol{\alpha}$ can be estimated as,

$$\hat{\boldsymbol{\alpha}} = (\boldsymbol{X}^{\mathrm{T}}\boldsymbol{X})^{-1}\boldsymbol{X}^{\mathrm{T}}\boldsymbol{y}\,. \quad (27)$$

The variance $\sigma^2$ can be estimated as,

$$\hat{\sigma}^2 = \frac{1}{(K-1)}(\boldsymbol{y} - \boldsymbol{X}\hat{\boldsymbol{\alpha}})^{\mathrm{T}}(\boldsymbol{y} - \boldsymbol{X}\hat{\boldsymbol{\alpha}}). \quad (28)$$

The estimation results are shown in **Table 8**. Because of the limited space of the vehicle interior, the test can only measure the path loss at distances smaller than 2.3 meter, which is not enough for reliable path loss exponent or large scale fading estimation. However, the results are provided for completeness under the assumption of in-vehicle communication.

**Table 8: Path loss parameter estimation for measured data**

| | $P_{\mathrm{L}}(d_0)$ | $n$ | $\sigma$ |
|---|---|---|---|
| Indoor LOS | 70.36 dB | 2.04 | 0.63 |
| Indoor NLOS | 82.42 dB | 1.55 | 1.77 |

### 4.5.4 Communication performance in test Scenario 3

The measurement in this scenario is to check the feasibility of this standard for the vehicle-to-infrastructure communication. The measurement results are presented in **Figure 34**.

When the vehicle's transceiver (**transceiver B**) is placed on the external roof, the high throughput communication is achievable. Moreover, the quality of the communication is perfect in terms of low packet error rate. However, as the transceiver distance increases, the average data throughput drops down from 888 Mbps at 0.9m to 305 Mbps at 10.0m, which is the maximum distance between vehicle front end and the outdoor service point with current EVBs. In practice, the link range can be further improved with higher output power or a different antenna design.

However, when **transceiver B** is moved inside the vehicle, the performance becomes worse. The maximum distance between the vehicle front end and the outdoor service point reduces to be only 1.1 meters, with an average data throughput of only 300 Mbps. The reason for the performance degradation can be found in **Table 9**. The comparison between the measured RCPI values in two situations indicates that the signal suffers more than 10 dB path loss when penetrating through the front windshield, which finally resulting in the reduction in SNR. At certain distance, the lower SNR leads to decrement in data throughput. When applying a fixed modulation scheme, the lower SNR determines the shorter link range.

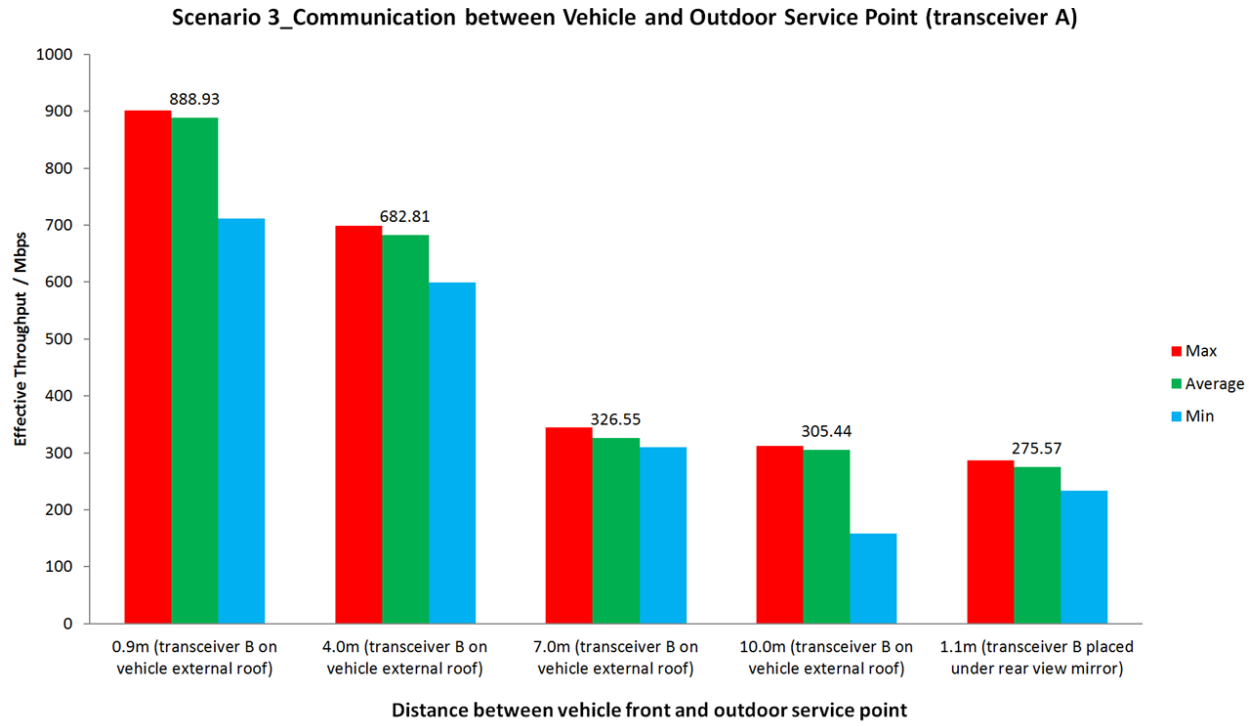


(a) MAC layer data throughput

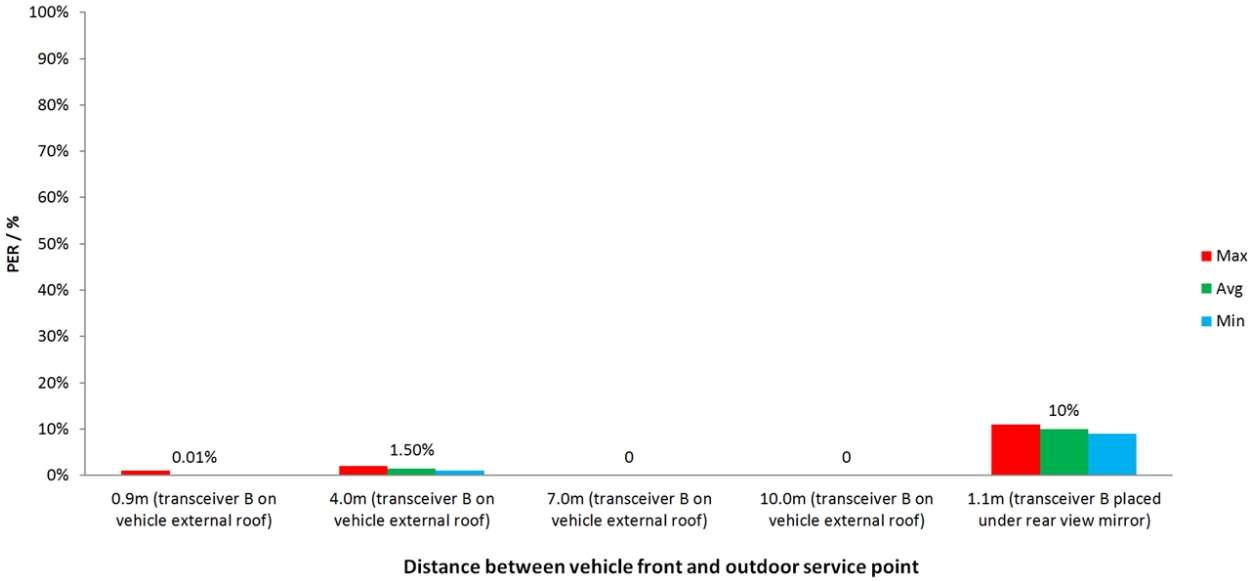


(b) Packet Error Rate

**Figure 34: Measured communication performance in Scenario 3**

**Table 9: The measured RCPI in two different test cases**

| Transceiver B Position | Distance | Max | Min | Median | Average |
|---|---|---|---|---|---|
| On the external roof. | 0.9 meter between vehicle front end and transceiver A | -64 dBm | -67 dBm | -65 dBm | -65.4 dBm |
| Under the rear view mirror inside vehicle | 1.1 meter between vehicle front end and transceiver A | -74 dBm | -78 dBm | -75 dBm | -75.5 dBm |

## 4.6 Discussion

### 4.6.1 Path loss parameters estimation

The path loss parameters are estimated based on the measured RCPI. Since the focus is mainly on the in-vehicle communication, 2.3 meter might be the maximum useable distance. Under this assumption, the results in Section **4.5.3** are fine.

### 4.6.2 Data throughput

According to the data sheet from the transceiver supplier, the designed maximum data throughput on MAC layer of the EVKs is only around 1.03 Gbps. The communication system doesn't achieve the full potential of the standard. There may be multiple reasons for this problem. First, the clock frequency of the EVBs only supports data rates up to 1.6 Gbps on physical layer. The connectivity by USB 3.0 between EVB and laptop might be the bottleneck for higher throughput due to, perhaps, the imperfect compatibility between drivers. At the bench test stage, sometimes the data throughput couldn't be over 800 Mbps no matter how good the channel condition was. A much higher data throughput (over 1.03Gbps) is recorded by the supplier when the measurement is performed directly on the boards. The last explanation might be that there is no algorithm to optimize the allocation of resources (e.g. CPU, memory) in the computer when processing the very high throughput data transferring task.

### 4.6.3 Antennas

The EVBs apply the integrated quasi-directional antennas. It only takes up small space but can achieve a large antenna gain.

For outdoor communication, the antenna works well. Its coverage angle is enough to satisfy the requirement and its high antenna gain ensures an acceptable link range for practical application. If more antenna radiating elements are applied with the beamforming technology, coverage angle can be further enlarged with higher antenna gain, which may bring more flexibility in practice.

However, for indoor communication, the observations during test indicate many limitations of this antenna. The vehicle interior is a small closed space but full of different kinds of obstacles, such as human bodies, leather seats with metal frame, glass objects. But due to the propagation features of 60 GHz signal, it's difficult for the signal to penetrate these objects. Moreover, because of the shorter wavelength, the surface of reflecting objects appears to be "rougher", which leads to less direct reflection of the signal but greater diffusion reflection. Apart from the LOS link, inside the vehicle the received power is mostly from the reflection on the "smooth" objects, like skylight or windshield. As a result, the multi path effect might be weak. Therefore, for interior vehicle communication, it's necessary to set up the LOS channels in different directions, which means that an omni-directional antenna or a phased array antenna with beamforming technology is more suitable. If the cost is not the problem, the latter one is preferred, which can improve the coverage performance without the sacrifice on antenna gain.

In addition, the linear polarization of the antenna also limits its performance for vehicle-to-device communication. If the polarization plane of antennas at both sides are not the same, the received signal may lose more power (even lose the whole power if polarization planes are orthogonal) at antenna end. This problem is clearly shown by the measurement results over time samples in test case "Front right seat" in Scenario 1.1 (as visible in **Figure 35**). In this case, we imitate the situation of using a hand held device in vehicle. We did some rotation and vibration on transceiver B, so during different time period the polarization plane of transceiver B was at different angle with respect to the polarization plane of transceiver A. The results show the communication system is very sensitive to these changes. Sometimes, the data throughput was about 230 Mbps, but at serval occasions it dropped down to only 60 Mbps. At some specific orientation, the communication was even unavailable.

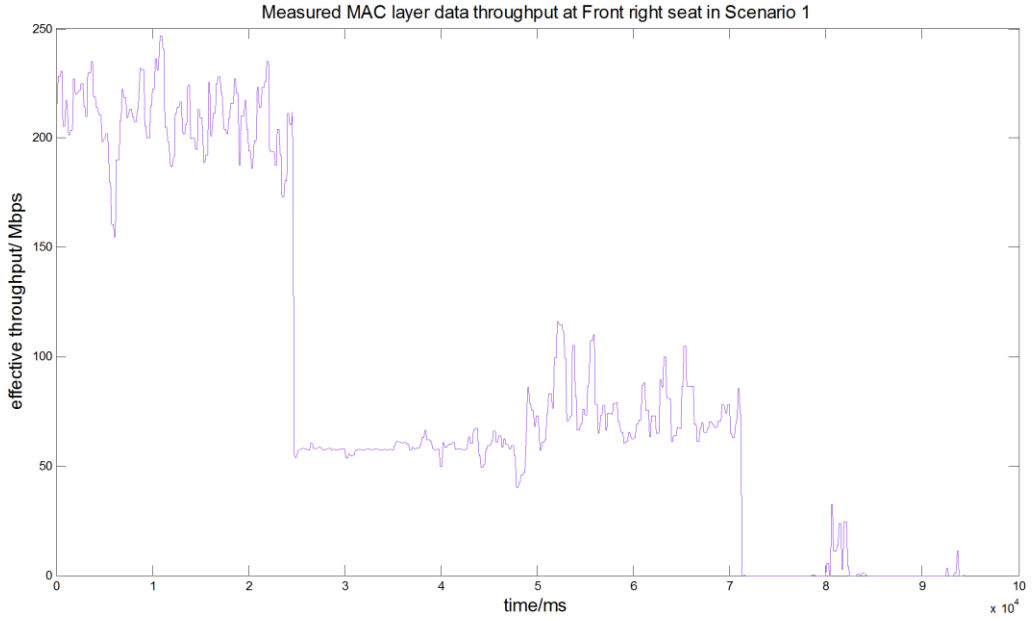


**Figure 35: Measured data throughput at front right seat**

### 4.6.4 Practical application

As presented in Section **4.5**, the high throughput communication could be achieved in vehicle with the standard IEEE 802.11ad. Moreover, the large penetration loss through vehicle body (windshield, and door) ensures that the communication inside different vehicles won't interfere with each other even when the vehicles are very close to each other. As a result, this standard enables us to implement the emerging applications or the service with high data rate requirement. Additionally, the measurement results also show that placing the WLAN hot spot near the position of central speaker or the rear ceiling may guarantee better performance of these applications or service.

However, due to the bad penetration ability and diffuse reflection of vehicle interior, the reliable and high quality communication is only available at some specific positions inside the vehicle. Although as discussed in the Section **4.6.3**, the coverage ability can be improved with more suitable antenna design, the effects of passenger's body and device movement can't be avoided. Therefore, unlike other conventional standards (802.11 a/b/n) working in lower frequency bands, it's not practical to cover the whole area inside the vehicle with one WLAN hot spot when applying the WLAN standard IEEE 802.11ad. Placing multiple WLAN hot spots inside the vehicle might be an option to enlarge coverage area in the future, while the cost is a show stopper at the current stage.

It will be valuable for the applications that require transferring the large files in the future. However, the limited link range determines that it's practical to apply the standard for outdoor communication only when the vehicle stands still.

# Chapter 5

# Practical implementation

This Chapter will present the basic plan for the implementation of IEEE 802.11ad for V2X communication. This plan includes the use cases based on the results from Chapter 3 and Chapter 4, the basic requirements on the core hardware components, the necessary test tools and the potential equipment vendors.

## 5.1 Use cases

This part introduces use cases of IEEE 802.11ad in vehicle. These use cases are based on the previous results and the advantages of this standard, such as high data throughput and low interference band.

1. Intra-vehicle entertainment
   The transmission of HD multimedia data, especially the uncompressed multimedia streaming (e.g. the online uncompressed 1080p video requires the data rates up to 2.98 Gbps) inside the vehicle can be achieved inside the vehicle. The passengers can enjoy their favorite movies or TV shows in high definition quality without any annoying cables. The zero-lag wireless interacted gaming may be another entertainment option for the passengers.

   In addition, if the holography 3D is matured to the market, it can also be supported by this standard in terms of data rate.

   *Constraints:* The performance highly depends on the processing speed of CPU and the memory performance at application terminals. Besides, the power consumption is important to care about

2. Software update, Map downloading
   The high capacity of IEEE 802.11ad enables transferring of the file of large size in a very short span of time, such as operating systems, navigation maps especially the ones for driverless car in the future. When pulling over near a service point, the download or the update of above information will be done in a short period of time.

   *Constraints:* The short communication range may limit the usage of these services. The performance of storage drive (especially the read/write speed), CPU, memory will affect practical communication performance.

3. Communication between ECUs
   The weight of wired communication system of vehicle has been increasing due to more and more ECUs. This trend conflicts human efforts on energy saving and environment protection. What's worse, as the number of ECUs increases, the design of wiring becomes much more complex. The standard IEEE 802.11ad may offer new solution to such problems. The high capacity satisfies the requirement on the data rates while low latency and low interference ensure the reliability.

   However, according to the test results, at current stage a complete wireless solution is not practical. Meanwhile, the research results in **[29]** indicate an interesting alternative option. It can be considered as a hybrid of wired and wireless communication, because it applies small horn antenna and one kind of waveguide as the communication channel. The measured results of latency, transmission loss and data throughput in different conditions (e.g. the waveguide is cut or pinched) verify its validity. Moreover, multi-channel communication is available on one waveguide. It can reduce the conventional cable weight to $\frac{1}{10}$, which is meaningful for reducing the fuel consumption. Therefore, it's valuable to keep an eye on the further development of this technology, but now the cost of the waveguide is the biggest challenge.

## 5.2 Practical implementation

### 5.2.1 Antenna

Because the devices inside the vehicle or the service infrastructure may appear in different orientation to the vehicle's access point, a larger angle of antenna coverage is necessary for the V2X communication. As discussed in the previous chapter, if not applying the antenna array, omni-directional antennas should be the best choice for most use cases. **Table 10** shows a list of 60 GHz antennas which can be used in vehicles.

Because of the very large attenuation loss of the antenna cable at this high operating frequency, it's better to embed the antennas together with the transceivers at current stage. But in the near future, as the cost is reduced, a small loss waveguide can be used for the connection between the antenna and transceivers. Moreover, in this way, it may be possible to integrate 60 GHz antennas together with the antennas designed for other bands. The results in **[29]** shows that the metal coated plastic pipe waveguide (radius = 6.5mm) only has the attenuation loss of 8.2 dB/m. In **[30]**, another rectangular waveguide (width a = 2mm and height b = 1mm) is researched. The material is solid plastic (Rogers RO3006) with dielectric constant of 6.15. The attenuation loss is only 2.33 dB/m. According to these results, it's valid to apply the waveguide for IEEE 802.11ad. However, as mentioned before, now the cost of waveguide cable is the show stopper here.

**Table 10: 60 GHz antennas (Source: [19] [20])**

| Product ID | Direction Type | Antenna Gain (dBi) | Beam pattern (degree) | Size (cm×cm×cm) |
|---|---|---|---|---|
| PE-W15A001 | Omni-directional | 0 | 360(Horizontal), 35(vertical) | 10(diameter) |
| SAO-5836230230-15-s1 | Omni-directional | 2 | 360(Horizontal), 30(vertical) | 10.2(diameter) |
| PE9881-20 | Directional Horn | 20 | 20 | 4.5×2.7×2.7 |
| PE9881-24 | Directional Horn | 24 | 12 | 4.8×4.5×2.9 |

### 5.2.2 Chipsets

The first IEEE 802.11ad product was launched to the market in 2014. The available chipsets are listed in **Table 11**. As can be seen, the development of chipsets is still at the early stage. Now, all the existing products only support the single carrier modulation. The full potential in data throughput hasn't been reached. Moreover, the beamforming technique is still away from its potential level.

**Table 11: Available chipsets for IEEE 802.11ad**

| Company | Product | Key features |
|---|---|---|
| Wilocity & Qualcomm | Wil6100 series | 4.6 Gbps throughput (MCS 0~12)<br>16 antenna elements |
| | Wil6200 series | 4.6 Gbps throughput (MCS 0~12)<br>32 antenna elements |
| SiBEAM | SB6510 & SB6501 | NA |
| Nitero | NT4600 | 4.6 Gbps throughput (MCS 0~12)<br>Android supported |
| Peraso | PRS4000 & PRS1025 | 4.6 Gbps throughput (MCS 0~12)<br>Windows, Linux, Android support |
| Tensorcom | TC60G1115GE SiP | 1.6 Gbps throughput (MCS 0~9)<br>2 antenna elements |

### 5.2.3 Hardware components surrounding transceiver

In theory, the maximum data rate is 6.75 Gbps, which sets up high requirements on hardware component surrounding the transceiver. First, the read/write speed of the storage solution should be at level of multi-gigabits per second. It's preferred to be over 6.75Gbps. The capacity of the storage should be large enough to store the files of large size (e.g. high definition movie, 3

dimension map). The physical dimension and the weight of the storage should be acceptable for the implementation in the vehicle. In addition, power consumption should be as small as possible. Currently, solid-state drive (SSD) especially some server storage may be solution to this problem. However, as can be seen in **Table 12**, no storage drive with high write/read speed can work in the environment below 0℃. As a result, a heater might be required near the storage drive.

Second, the internal wired connection between the transceiver and other components (e.g. HD screen, storage drive) must support high throughput transmission also. In terms of data rate, many mainstream computer bus in consumer industry can meet this target (shown in **Table 12**). Some of them may be the potential options. However, due to different requirements on the implementation in automotive, further research is needed.

**Table 12: SSD product examples**

| Company | Product | Read/Write speed (Gbps) | Interface | Weight (g) | Capacity (GB) | Power Idle/Active (w) |
|---|---|---|---|---|---|---|
| Intel | SSD 750 series | 17.6~19.2 / 7.2~9.6 | PCI-E | 125 | 1200 | 4/25 |
| | SSD 535 series | 4.3 / 3.9 | SATA | 78 | 480 | 0.06/0.17 |
| SanDisk | Lightning series | 2.4~8 / 1.1~4.8 | SAS | 238 | 400~1600 | 3.9/5.9 |
| | Optimus series | 4~4.4 / 3.0~4.3 | | NA | 400~4000 | NA/7 |
| | iSSD i110 | 2.8 / 3.6 | Integrated | 0.7 | 128 | 0.011/0.055 |
| | SATA series | 4.4 / 4~4.16 | SATA | NA | 960 | NA/0.15 |
| | Xseries | 4~4.2 / 3.7~3.8 | | 55~57 | 512 | 0.08/0.11 |
| | Ultra II | 4.4/4 | mSATA | NA | 512 | NA |
| | ULLtraDIMM | 7.04 / 4.8 | DDR3 | NA | 400 | 9/12.5 |
| ADATA | SX100L | 4.4/4 | SATA | 61 | 400 | 0.35/0.6 |
| | SR1010SS | 4.4/4.4 | SATA | 63 | 480 | 2.25/4.1 |
| | XPG SX series | 4.5/4.3 | SATA | 68 | 512 | 0.5/1.2 |
| | Premier Pro | 4.5 / 3.7~4.3 | SATA | 68 | 512~1000 | 0.06/0.2~0.6 |

**Table 13: Technologies for internal connection**

| Technology | Version | Transmission data rate (Gbps) |
|---|---|---|
| SATA | 2.0 | 2.4 |
| | 3.0 | 4.8 |
| | Express | 6.47 |
| SAS | Gen 1 | 3 |
| | Gen 2 | 6 |
| PCI-E | 1.0 X1 | 4 |
| | 1.0 X2 | 8 |
| PCI-X | 1.0 | 4.24~8.52 |
| Thunderbolt | 2.0 | 20 |

## 5.3 Testing tools

The test work is indispensable before launching any new product to the market. There should be at least two parts in the test of the implementation of one WLAN technology.

The first part is the acceptance test. The objective is to verify the product from the supplier fulfil the hard requirements defined in the standard (e.g. Transmit Mask, center frequency tolerance, etc.) and the hard requirements ruled by the government, like EIRP. Another objective is to check that the product satisfy the requirement from design group, including the parameters such as coverage angle, transmit power, working temperature and so on.

The second part is to certify that the performance meets the expectation and to provide the valuable feedback for the improvement of the design. The interested features include power consumption, link range, packet error rate, latency and data throughput.

The test tools for the measurement of different parameters (currently available) are shown in **Table 14**.

**Table 14: Testing tools**

| Measured Parameters | Available product |
|---|---|
| Transmit mask,<br>center frequency tolerance,<br>center frequency convergence,<br>transmit center frequency leakage<br>transmit rampup & rampdown,<br>flatness of OFDM frame,<br>EIRP | R&S® FSW67 signal and spectrum analyzer<br>Keysight 81199A-002 wideband waveform analyzer |
| Power consumption<br>Peak average ratio of OFDM frame | Keysight E8486A-201 waveguide power sensor<br>Keysight V8486A-H02 waveguide power sensor<br>Keysight N8488A thermocouple power sensor<br>R&S® NRP-Z57 thermal power sensor |
| | Keysight N1913A EPM single channel power meter<br>Keysight N1914A EPM dual channel power meter<br>R&S® NRP2 dual channel power meter |
| Working temperature, humidity | Thermotron SM-1.0 temperature and humidity chamber<br>CSZ MCB(H)-1.2 temperature and humidity chamber<br>Jeio tech. TH-ME-025 temperature and humidity chamber |
| Data throughput<br>Packet error rate<br>Latency | NA* |
| Link Range<br>Coverage angle | Laser rangefinder<br>Goniometer |

* Currently there is no product simulating the access point, so it's impossible to measure these parameters

# Chapter 6

# Conclusions

This thesis work studies the physical layer of the new WLAN standard IEEE 802.11ad. In this standard, the wireless communication signal is transmitted in the 60 GHz frequency band. The unprecedented large bandwidth promises very high data throughput exceeding 6 Gbps. The short wavelength implies small electronic components, which is beneficial in a MIMO system as more antenna radiating elements can be fitted into a given cross-section area. In addition, more choices of modulation schemes provide flexibility to meet different requirements, e.g. high data throughput, low power consumption or high robustness. On the other hand, due to inherent limitation at higher frequencies, the 60 GHz band suffers large path loss, high penetration loss and weak reflection gain, which may bring many problems in the practical implementation.

Therefore, in this thesis, the feasibility of this standard for V2X communication is investigated through theoretical analysis and practical test in a real vehicle. The results show that IEEE 802.11ad has an obvious advantage in data throughput over other existing WLAN standards, and that the performance is reliable at short distances in LOS channel. Moreover, the large penetration loss through the vehicle body implies that the interference between the indoor communications of different vehicles may be controlled at an acceptable level. These findings mean that the intra-vehicle multi-media streaming, high speed software update and large file downloading could be the use cases. However, the results also reveal the challenges in practical implementation of this standard, including large path loss, strong shadowing effect of human body and weak multi-path effect inside the vehicle. Further research on channel models for the vehicular environment, especially for the interior vehicle environment, is necessary.

In addition, this thesis work obtains valuable reference knowledge for future product design. We find that a linearly polarized quasi-directional antenna is not suitable for V2X communication, especially for vehicle-to-device communication. Instead, circularly polarized antennas should be the alternative plan. However, note that the system requires a phased array antenna with more than 2 radiating elements. We also find that the USB 3.0 isn’t reliable for the connection between transceiver and CPU. The solution need to be found among other computer bus technologies.

To sum up, this 60 GHz WLAN standard is promising and will bring new solutions to the future requirements on vehicles. It’s valuable to keep continuous attention to the development in this technology, especially the development of hardware components. But at the current stage of development, IEEE 802.11ad can only be considered as a complement of other wireless communication technology providing some specific service.

# References


[1] Volvo Car Corporation (2015, Dec.4), *Sensus Connect*. Retrieved from www.volvocars.com/intl/own/owner-info/sensus-connect.

[2] Cadillac Motor Car Division (2015, Dec. 4), *Onstar with 4G LTE* [Blog File]. Retrieved from www.cadillac.com/cadillac-cue/wifi-hotspot.html

[3] IEEE Computer Society, "IEEE standard for IT - telecommunications and information exchange between systems - LAN/MAN - specific requirements - part 11: Wireless LAN Medium Access Control (MAC) and Physical Layer (PHY)", IEEE Std 802.11™-2012, March 2012.

[4] IEEE Computer Society, "IEEE standard for IT - telecommunications and information exchange between systems - LAN/MAN - specific requirements - part 11: Wireless LAN Medium Access Control (MAC) and Physical Layer (PHY) Specifications: High-speed Physical Layer in the 5 GHz band," IEEE Std 802.11a™-1999, 1999.

[5] IEEE Computer Society, "IEEE standard for IT - telecommunications and information exchange between systems - LAN/MAN - specific requirements - part 11: Wireless LAN Medium Access Control (MAC) and Physical Layer (PHY) Specifications: High-speed Physical Layer Extension in the 2.4 GHz Band," IEEE Std 802.11b™-1999, September 1999.

[6] IEEE Computer Society, "IEEE standard for IT - telecommunications and information exchange between systems - LAN/MAN - specific requirements - part 11: Wireless LAN Medium Access Control (MAC) and Physical Layer (PHY) Specifications: Further Higher Data Rate Extension in the 2.4 GHz Band," IEEE Std 802.11g™-2003, July 2003.

[7] IEEE Computer Society, "IEEE standard for IT - telecommunications and information exchange between systems - LAN/MAN - specific requirements - part 11: Wireless LAN Medium Access Control (MAC) and Physical Layer (PHY) Specifications - Amendment 5: Enhancements for Higher Throughput," IEEE Std 802.11n™-2009, November 2009.

[8] IEEE Computer Society, "IEEE standard for IT - telecommunications and information exchange between systems - LAN/MAN - specific requirements - part 11: Wireless LAN Medium Access Control (MAC) and Physical Layer (PHY) Specifications - Amendment 4: Enhancements for very high throughput for Operation in Bands below 6 GHz," IEEE Std 802.11ac™-2013, December 2013.

[9] IEEE Computer Society, "IEEE standard for IT - telecommunications and information exchange between systems - LAN/MAN - specific requirements - part 11: Wireless LAN Medium Access Control (MAC) and Physical Layer (PHY) Specifications - Amendment 3: Enhancements for very high throughput for in the bands 60 GHz Band," IEEE Std 802.11ad™-2012, December 2012.

[10] Rohde & Schwarz, *802.11ad – WLAN at 60 GHz a technology introduction White Paper*, Munich Germany, 1MA220_1e, Nov. 2013. [Online] Available: www.rohde-schwarz.com /en/application/802.11ad-wlan-at-60-ghz-application-note_56280-50625.html

[11] Federal Communications Commissions, *Revision of Part 15 of the Commission's Rules Regarding Operations in the 57-64 GHz Band*, Washington D.C., 2013.

[12] S.K. Yong, P. Xia, A. Garcia, "60 GHz Technology for GBPS WLAN and WPAN from Theory to Practice", John Wiley and Sons Ltd, 2011

[13] Federal Communications Commissions, *Millimeter Wave Propagation: Spectrum Management Implications*, Washington D.C., 1997.

[14] C. Gustafson, "60 GHz Wireless Propagation Channels: Characterization, Modeling and Evaluation*"*, Ph.D. thesis, Department of Electrical and Information Technology, Lund University, Lund, Sweden, 2014.

[15] T. S. Rappaport, E. Ben-Dor, J. N. Murdock, Y. Qiao, "38 GHz and 60 GHz Angle-dependent Propagation for Cellular & Peer-to-Peer Wireless Communications", *IEEE International Conference on Communication*, Ottawa, Canada, June 2012.

[16] P. F. M. Smulders, "Statistical Characterization of 60-GHz Indoor Radio Channels", *IEEE Transactions on Antenna and Propagation*, VOL. 57, No. 10, October 2009.

[17] J. P. Linnartz, "Radio Propagation Model" in *Wireless Communication, The Interactive Multimedia CD-ROM*, Vol. 1, Amsterdam: Baltzer Science Publisher, 1996

[18] P. Kyosti, J. Medbo, A channel model for 5G evaluations, Deliverable D1.4 METIS Channel Models, Mobile and wireless communications Enablers for the Twenty-twenty Information Society, April, 2015

[19] Pasternack, "Omni-directional Antenna operating from 58 GHz to 63 GHz with a nominal 0dBi gain and WR-15 waveguide input", PE-W15A001 data sheet, 2014 [Received May 2015].

[20] SAGE Millimeter, Inc., "V-Band Omni-Directional Antenna", SAO-5836230230-15-S1 data sheet, Sep. 2014 [Received May 2015].

[21] P. Jensen, "IEEE conference: more stream for 60 GHz wireless", *The Netze Network news,* week 21, 2014. [Online], Available: www.heise.de/netze

[22] X. Zhu, A. Doufexi, T. Kocak, "Beamforming Performance Analysis for OFDM Based IEEE 802.11ad Millimeter-Wave WPANs", *8th International Workshop on Multi-Carrier Systems & Solutions (MC-SS),* May 2011, Herrsching, Germany.

[23] Y. Blankenship, P. Sartori, B. Classon, and K. Baum, "Link Error Prediction Methods for Multicarrier Systems", *IEEE 60th Vehicular Technology Conference,* Sep. 2004, Los Angeles, USA.

[24] IEEE Computer Society, "IEEE standard for IT - telecommunications and information exchange between systems - LAN/MAN - specific requirements - part 15.3: Wireless Medium Access Control (MAC) and Physical Layer Specifications for High Rate Wireless Personal Area Networks (WPANs) - Amendment 2: Millimeter-wave-based alternative physical layer extension", IEEE Std 802.15.3c™-2009, Oct. 2009.

[25] IEEE P802.15 Working Group, IEEE P802.15-08-0355-00-003c, May 2008.

[26] S. Yoon, T. Jeon and W. Lee, "Hybrid Beam-forming and Beam-switch for OFDM Based Wireless Personal Area Network", *IEEE Journal on Selected Areas in Communications,* Vol. 27, Issue 8, pp. 1425-1432, October 2009.

[27] Volvo Car Group Global Newsroom (2014, Aug.27), *The all new Volvo XC90* [Image file]. Retrieved from www.media.volvocars.com/global/en-gb/models/all-new-xc90/2016/photos

[28] T. Abbas, C. Gustafson and F. Tufvesson, "Pathloss Estimation Techniques for Incomplete Channel Measurement Data", *European Cooperation in the field of Scientific and Technical research,* May 2014, Aalborg, Denmark.

[29] Y. Sato, V. Ith and S. Kato, "60GHz Radio Hose for Wireless Harness Communication System", *The Eighth International Conference on Sensor Technologies and Applications,* Nov. 2014, Lisbon, Portugal.

[30] S. Fukuda, Y. Hino, S. Ohashi, T. Takeda, H. Yamagishi, S. Shinke and K. Komori, "A 12.5+12.5 Gb/s Full-Duplex Plastic Waveguide Interconnect", *IEEE Journal of Solid-State Circuit and,* VOL. 46, No. 12, December 2011.

# Appendix A

# Test Plan

## A.1 Definition

### A.1.1 Problem statement

See details in **4.1.1**.

### A.1.2 The factors involved

The factors that affect the feasibility of implementing the standard IEEE 802.11ad for V2X communication can be divided into two groups: input factors and output factors. And a relationship y= f(x) can be set up between these two groups.

**Table A- 1: Input factor and Output factor Matrix**

| Output factor (y) / Input factor (x) | Link range | Data Throughput | Frame error rate | Rx_SNR | Latency |
|---|---|---|---|---|---|
| Antenna Location (Inside/Outside) | × | × | × | × | |
| Antenna Location (Front/Middle/Rear) | × | × | × | × | |
| Passenger Density | × | × | × | × | × |

(× means the output factor has relations with input factor)

### A.1.3 Test scope

See details in **4.1.2**.

## A.2 Time plan

**Table A- 2: Time table for the test**

| Test kickoff | Day 1 | Day 2 | Day 3 | Day 4 | Day 5 | Day 6 | Day 7 | Day 8 |
|---|---|---|---|---|---|---|---|---|
| **Prepare** | $\frac{1}{2}$ day | | | | | | | |
| **Measure** | $\frac{1}{2}$ day | × | × | $\frac{1}{2}$ day | | | | |
| **Analysis** | | | | $\frac{1}{2}$ day | × | × | × | |
| **Discussion** | | | | | | | | $\frac{1}{2}$ day |
| **Results presentation** | | | | | | | | $\frac{1}{2}$ day |

## A.2 Test roles

**Table A- 3: Responsibility definition for the test participants**

| Roles | Responsibility |
|---|---|
| **Test engineer** | • Develop test plan<br>• Analysis of test results (Day 4) |
| **Base technology engineer** | • Allocate necessary equipment and record their condition (Day 1)<br>• Execute the tests according to test plans (Day 1)<br>• Document tests results (Day 4) |
| **Technical expert** | • Review test results (Day 5)<br>• Provide feedback on improvements of test plan (Day5) |
| **Internal customers** | • Review the test summary (Day 6) |

## A.3 Test Environment

See details in **4.2**.

## A.4 Data Collection

### A.4.1 Data collection approach

The data is collected from the software shown in **Figure A- 1**.

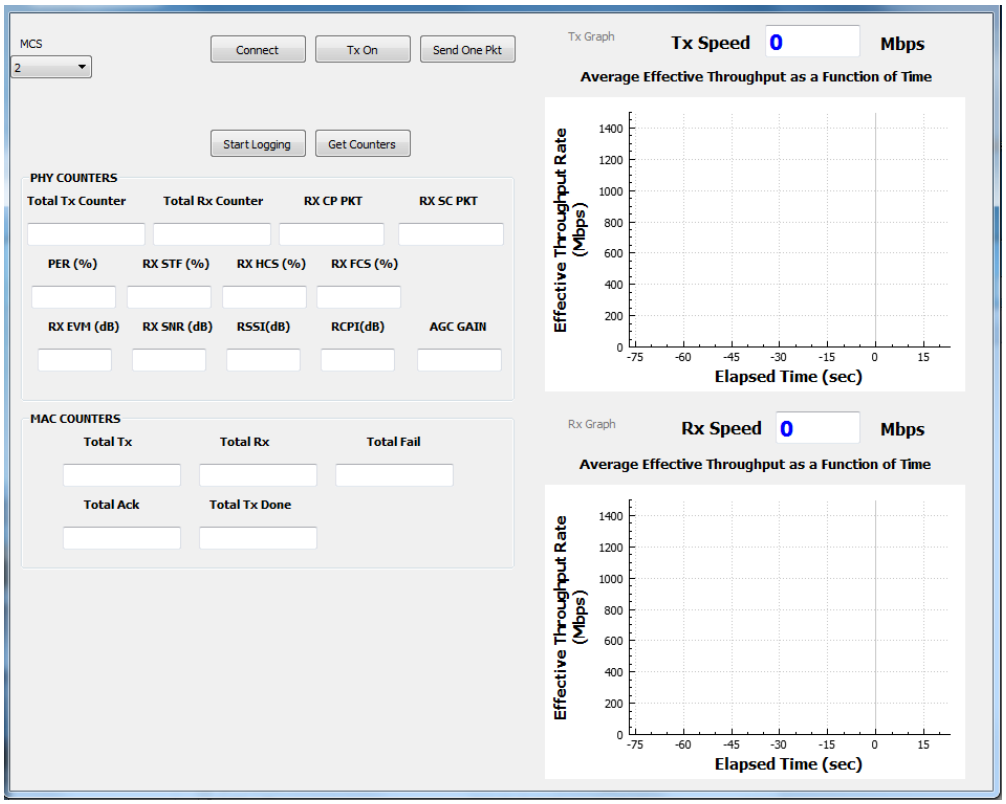


**Figure A- 1: The software GUI**

### A.4.2 Key data to be collected

See details in **4.3.1**.

### A.4.3 Possible causes on performance degradation in test

See details in **4.3.2**.

## A.5 Collection Plan

**Table A- 4: The list of necessary equipment**

| Object | Description | Status [ ok / not ok] |
|---|---|---|
| **Scheduled test location** | Schedule suitable test location for the test suite. | |
| **Vehicle** | One new XC 90 | |
| **USB 3.0 super speed cable** | Arrange 2 cables that shall be used for the connection between laptop and evaluation board with correct length. | |
| **Wi-Fi evaluation boards** | Two TC60G-USB3.0 Evaluation Kits from Tensorcom. The driver for it should be installed in laptops. | |
| **Analysis tool** | Install the software "Speedtest" to measure interested parameters | |
| **Internal Laptop** | Arrange 2 laptops with support for 5Gbps USB 3.0. The laptops shall have admin rights according to VCC IT policy. The operation system is Windows 7. | |
| **Desk top tripods** | Arrange 2 tripods to place the evaluation boards on desk top | |
| **Adhesive tape** | Arrange the tape to fix the evaluation board off the desk top | |
| **Laser rangefinder** | Arrange laser rangefinder to measure communication distance | |
| **Digital camera** | A camera shall be used to document the test-setup. | |

## A.6 Calibration Plan

Test engineer is responsible to calibrate the equipment.

**Table A- 5: Calibration sheet**

| Object | Description | Status [ ok / not ok] |
|---|---|---|
| **USB 3.0 cable** | Make sure that the cable is of good health and long enough | |
| **Cable fixer** | Check the fixer is tight enough | |
| **Analysis tool** | Make sure that the software is installed successfully. | |
| **Desk top tripods** | Make sure the tripods are of good health | |
| **Wi-Fi evaluation boards** | Make sure the evaluation boards are of good condition. The driver is installed successfully. | |
| **Digital Camera** | Make sure that there is enough free memory for pictures and the battery is fully charged. | |
| **Laptop** | Make sure that the laptop is in normal condition. Battery has a good status. Charge if needed. Arrange external power supply to the laptop. | |
| **Adhesive tape** | Check the tape has good stickiness | |
| **Laser rangefinder** | Make sure the tape is long enough and has clear scale | |
| **Vehicle** | Check the vehicle can work normally | |

## A.7 Test equipment check sheet

Laptops:

**Table A- 6: Parameters of test laptop**

| | Internal Laptop |
|---|---|
| **Brand:** | Dell |
| **CPU:** | Intel Core i7 |
| **Memory size:** | 8.00 GB |
| **USB interface:** | USB 3.0 SS |
| **OS:** | Win 7 64-bit enterprise |

Evaluation boards:

**Table A- 7: Parameters of evaluation boards**

| | |
|---|---|
| **Radio:** | 2 × 2 MIMO with beamforming |
| **Antenna type** | Endfire horizontally polarized (shown in **Figure A- 2**) |
| **Antenna coverage angle:** | +/- 30 degree horizontally, +/- 60 degree (visible in **Figure A- 3**) |
| **EIRP:** | 12.5 dBm |
| **Noise figure:** | 7.5 dB |
| **Implementation loss:** | 7.5 dB |
| **Transmission bandwidth:** | 1.76 GHz |
| **Antenna gain:** | 7.5 dBi |
| **Clock frequency:** | 100 MHz |

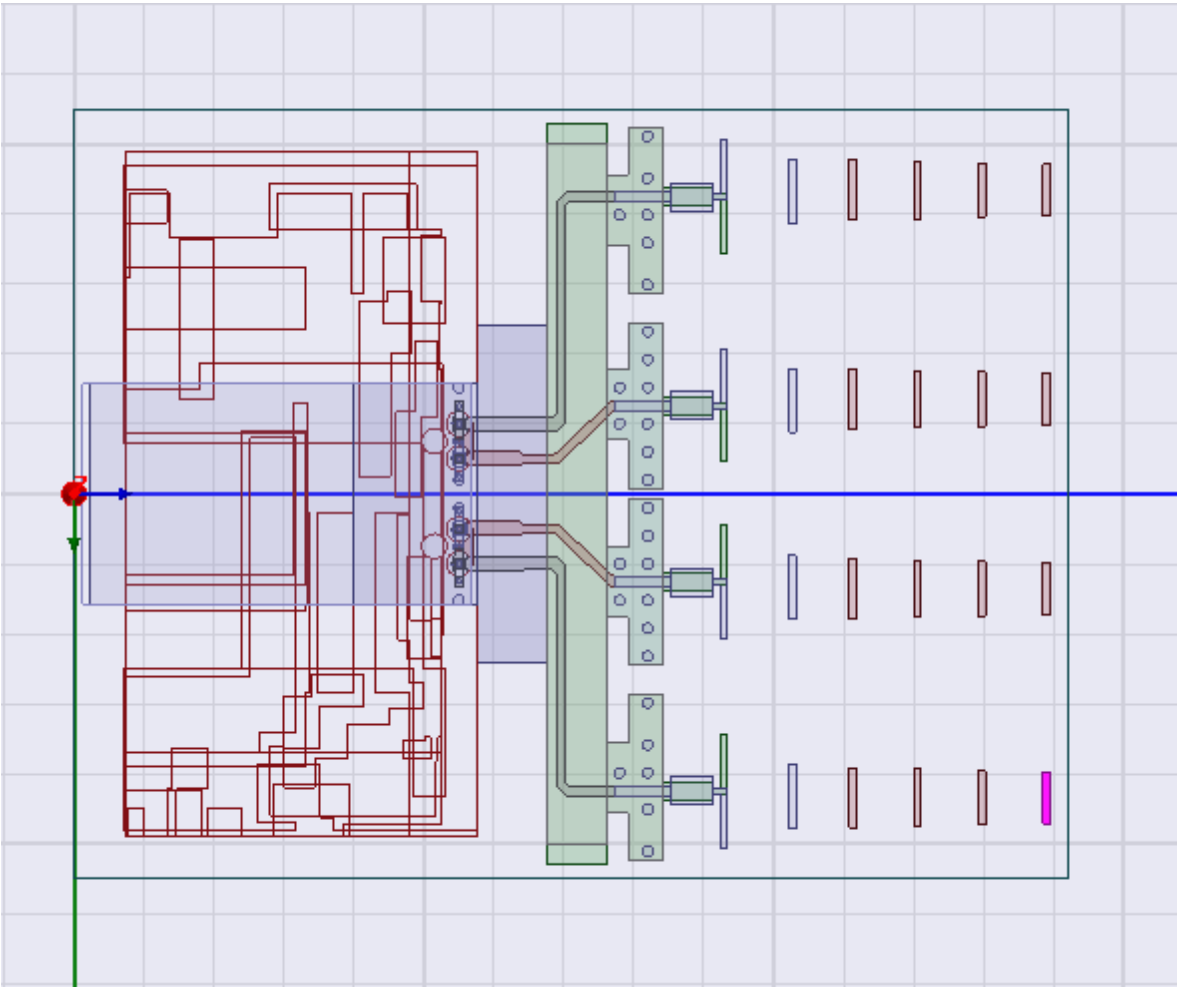

**Figure A- 2: The design graph of integrated antenna**

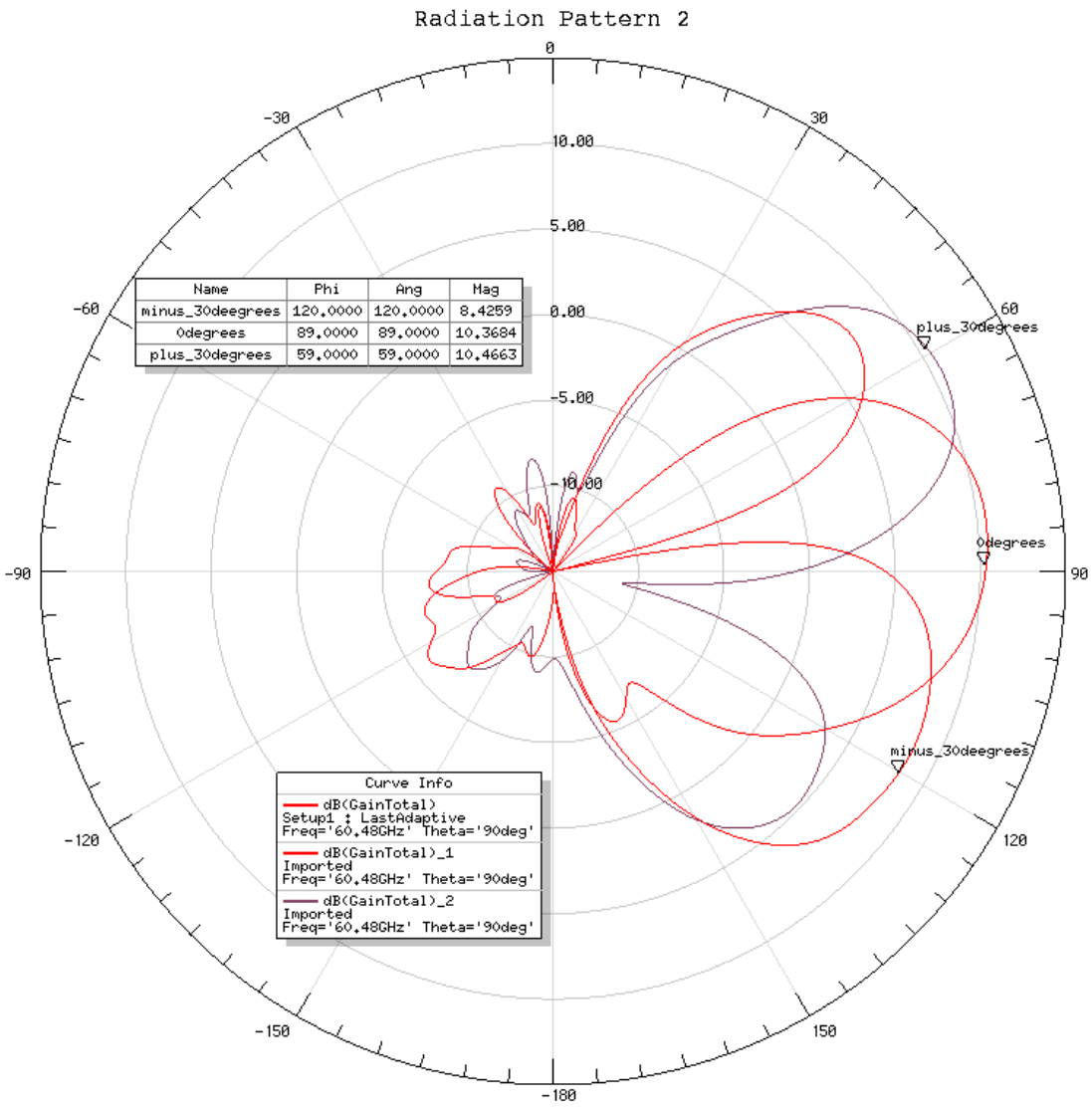


**Figure A- 3: The radiation plot of the antenna**

## A.8 Test configuration and Execution

### A.8.1 Test cases

The test cases are summarized in **Table A- 8**, covering different test scenarios.

**Table A- 8: The list of test cases**

| Test ID | Transceiver A position | Transceiver B position | Iteration | Duration |
|---|---|---|---|---|
| **1** | [red 1] the position of the central speaker | [blue 1] central display screen (CDS) | 5 | 30 sec |
| **2** | | [blue 2] front right seat | | |
| **3** | | [blue 3] backside of front right headrest | | |
| **4** | | [blue 4] backside of front left headrest | | |
| **5** | | [blue 5] rear right seat | | |
| **6** | | [blue 6] rear left seat | | |
| **7** | | [blue 7] rear left IC bone | | |
| **8** | | [blue 8] rear right IC bone | | |
| **9** | | [blue 9] the rear right side of trunk | | |
| **10** | [red 2] the position next to rear-view mirror | [blue 1] central display screen | | |
| **11** | | [blue 2] front right seat | | |
| **12** | | [blue 3] backside of front right headrest | | |
| **13** | | [blue 4] backside of front left headrest | | |
| **14** | | [blue 5] rear right seat | | |
| **15** | | [blue 6] rear left seat | | |
| **16** | | [blue 7] rear left IC bone | | |
| **17** | | [blue 8] rear right IC bone | | |
| **18** | | [blue 9] the rear right side of the trunk | | |
| **19** | [red 3] the rear ceiling | [blue 1] central display screen | | |
| **20** | | [blue 2] front right seat | | |
| **21** | | [blue 3] backside of front right headrest | | |
| **22** | | [blue 4] backside of front left headrest | | |
| **23** | | [blue 5] rear right seat | | |
| **24** | | [blue 6] rear left seat | | |
| **25** | | [blue 9] the rear right side of the trunk | | |
| **26** | [blue 1]central display screen | [blue 9] the rear right side of the trunk | | |
| **27** | [red 4] the external roof of the vehicle | [blue10] outdoor service point on the platform at height of 2m from ground | | |
| **28** | [red 5] the position below rear view mirror | [blue10] outdoor service point on the platform at height of 2m from ground | | |

### A.8.2 Test configuration

**Table A- 9: The default configuration for the test**

| | |
|---|---|
| Test vehicle | The new Volvo XC 90 D5 |
| Passengers | One driver, one passenger on the rear left seat |
| Indoor Temperature | 20.5 $^0$C at front seat, 22.5 $^0$C at rear seat |
| Vehicle condition | Stand still but the engine on |

### A.8.3 Test execution in Scenario 1 & 2

See details in **4.4.1**.

### A.8.4 Test execution in Scenario 3

See details in **4.4.2**.

### A.8.5 6 sigma process of test execution

See details in **4.4.3**.